

# CD8<sup>+</sup> T cells regulate tumour ferroptosis during cancer immunotherapy

Weimin Wang<sup>1,2</sup>, Michael Green<sup>2,3</sup>, Jae Eun Choi<sup>2,4,5</sup>, Miguel Gijón<sup>6</sup>, Paul D. Kennedy<sup>6</sup>, Jeffrey K. Johnson<sup>6</sup>, Peng Liao<sup>1,2</sup>, Xueling Lang<sup>1,2,3</sup>, Ilona Kryczek<sup>1,2</sup>, Amanda Sell<sup>1,2</sup>, Houjun Xia<sup>1,2</sup>, Jiajia Zhou<sup>1,2</sup>, Gaopeng Li<sup>1,2</sup>, Jing Li<sup>1,2</sup>, Wei Li<sup>1,2</sup>, Shuang Wei<sup>1,2</sup>, Linda Vatan<sup>1,2</sup>, Hongjuan Zhang<sup>1,2</sup>, Wojciech Szeliga<sup>1,2</sup>, Wei Gu<sup>7</sup>, Rebecca Liu<sup>8</sup>, Theodore S. Lawrence<sup>3</sup>, Candice Lamb<sup>9,10</sup>, Yuri Tanno<sup>9,10</sup>, Marcin Cieslik<sup>4,11</sup>, Everett Stone<sup>9,10</sup>, George Georgiou<sup>9,10</sup>, Timothy A. Chan<sup>12</sup>, Arul Chinnaiyan<sup>4,5,13</sup> & Weiping Zou<sup>1,2,4,14,15\*</sup>

**Cancer immunotherapy restores or enhances the effector function of CD8<sup>+</sup> T cells in the tumour microenvironment<sup>1,2</sup>. CD8<sup>+</sup> T cells activated by cancer immunotherapy clear tumours mainly by inducing cell death through perforin–granzyme and Fas–Fas ligand pathways<sup>3,4</sup>. Ferroptosis is a form of cell death that differs from apoptosis and results from iron-dependent accumulation of lipid peroxide<sup>5,6</sup>. Although it has been investigated in vitro<sup>7,8</sup>, there is emerging evidence that ferroptosis might be implicated in a variety of pathological scenarios<sup>9,10</sup>. It is unclear whether, and how, ferroptosis is involved in T cell immunity and cancer immunotherapy. Here we show that immunotherapy-activated CD8<sup>+</sup> T cells enhance ferroptosis-specific lipid peroxidation in tumour cells, and that increased ferroptosis contributes to the anti-tumour efficacy of immunotherapy. Mechanistically, interferon gamma (IFN $\gamma$ ) released from CD8<sup>+</sup> T cells downregulates the expression of SLC3A2 and SLC7A11, two subunits of the glutamate–cystine antiporter system x<sub>c</sub><sup>-</sup>, impairs the uptake of cystine by tumour cells, and as a consequence, promotes tumour cell lipid peroxidation and ferroptosis. In mouse models, depletion of cystine or cysteine by cyst(e)inase (an engineered enzyme that degrades both cystine and cysteine) in combination with checkpoint blockade synergistically enhanced T cell-mediated anti-tumour immunity and induced ferroptosis in tumour cells. Expression of system x<sub>c</sub><sup>-</sup> was negatively associated, in cancer patients, with CD8<sup>+</sup> T cell signature, IFN $\gamma$  expression, and patient outcome. Analyses of human transcriptomes before and during nivolumab therapy revealed that clinical benefits correlate with reduced expression of SLC3A2 and increased IFN $\gamma$  and CD8. Thus, T cell-promoted tumour ferroptosis is an anti-tumour mechanism, and targeting this pathway in combination with checkpoint blockade is a potential therapeutic approach.**

To study whether ferroptosis is involved in the anti-tumour activity of cancer immunotherapy, we treated mice bearing ovarian tumours derived from ID8 cells with programmed death-ligand 1 (PD-L1) blockade, and assessed lipid peroxidation as a functional marker for ferroptosis<sup>5,11</sup> in single cells. PD-L1 blockade therapy resulted in increased lipid reactive oxygen species (ROS) in CD45<sup>-</sup> ID8 cells (Fig. 1a, Extended Data Fig. 1a), but not in CD45<sup>+</sup> cells (Extended Data Fig. 1a), and reduced tumour growth (Fig. 1b, Extended Data Fig. 1b). Similarly, PD-L1 blockade increased lipid ROS in CD45<sup>-</sup> tumour cells (Fig. 1c) and reduced tumour weight (Fig. 1d) in mice bearing subcutaneous melanomas derived from B16 cells. Adoptive transfusion

of ovalbumin (OVA)-specific CD8<sup>+</sup> T (OT-I) cells into mice bearing OVA<sup>+</sup> B16 tumours also increased lipid ROS in CD45<sup>-</sup>OVA-H2K<sup>b</sup><sup>+</sup> tumour cells (Fig. 1e, Extended Data Fig. 1c), but not in CD45<sup>+</sup> cells (Extended Data Fig. 1d). The increased lipid peroxidation in tumour tissues from mice transfused with OT-I cells was further confirmed using a malondialdehyde (MDA) assay (Extended Data Fig. 1e). In addition, OT-I cells reduced tumour growth (Fig. 1f, Extended Data Fig. 1f).

To further explore whether the increased lipid ROS and ferroptosis contribute to the efficacy of cancer immunotherapy, we generated erastin-resistant (Erastin<sup>resis</sup>) ID8 cells, which were insensitive to rechallenge with erastin or RSL3, another inducer of ferroptosis (Extended Data Fig. 2a), but remained sensitive to doxorubicin and gemcitabine, two inducers of apoptosis, as compared to parental cells in vitro (Extended Data Fig. 2b). In vivo, in contrast to the parental cells, Erastin<sup>resis</sup> ID8 cells did not respond efficiently to PD-L1 blockade (Extended Data Fig. 2c). Similarly, PD-L1 blockade failed to increase lipid ROS in RSL3-resistant (RSL3<sup>resis</sup>) B16 cells or to decrease tumour weight in mice bearing tumours derived from RSL3<sup>resis</sup> B16 cells (Extended Data Fig. 2d–g). Moreover, we tested the effect of the ferroptosis inhibitor liproxstatin-1 on the efficacy of checkpoint blockade in vivo<sup>12</sup>. The combination of the checkpoint blockers anti-CTLA-4 and anti-PD-L1 efficiently reduced B16 tumour growth, and this effect was attenuated by liproxstatin-1 (Fig. 1g). A recent report showed that long-chain-fatty-acid-CoA ligase 4 (ACSL4) has a key role in ferroptosis<sup>8</sup>. ACSL4 levels were reduced in both Erastin<sup>resis</sup> ID8 and RSL3<sup>resis</sup> B16 cells (Extended Data Fig. 2h). We generated ACSL4<sup>-/-</sup> ID8 cells and found that they were resistant to cell death induced by erastin or RSL3 in vitro (Extended Data Fig. 2i, j). Wild-type but not ACSL4<sup>-/-</sup> ID8 tumours responded effectively to PD-L1 blockade in vivo (Extended Data Fig. 2k, l).

We investigated whether immunotherapy-activated CD8<sup>+</sup> T cells could directly affect cancer cell ferroptosis. In a co-culture of OVA<sup>+</sup> tumour cells with OT-I cells, activated OT-I cells enhanced lipid ROS in B16 cells (Fig. 1h) and augmented RSL3-induced cell death in ID8 (Extended Data Fig. 2m) or B16 cells (Fig. 1i), and these effects were reversed by ferrostatin-1 (Fig. 1i). However, in the absence of RSL3, ferrostatin-1 did not rescue OT-I cell-induced death of OVA<sup>+</sup> B16 cells in vitro (Extended Data Fig. 2n). Supernatant from activated mouse CD8<sup>+</sup> T cells could increase lipid ROS in B16 and ID8 cells (Fig. 1j). Similarly, supernatant from activated human CD8<sup>+</sup> T cells increased lipid ROS in HT-1080 cells (a human sarcoma cell line; Fig. 1k) and

<sup>1</sup>Department of Surgery, University of Michigan School of Medicine, Ann Arbor, MI, USA. <sup>2</sup>Center of Excellence for Cancer Immunology and Immunotherapy, University of Michigan Rogel Cancer Center, University of Michigan School of Medicine, Ann Arbor, MI, USA. <sup>3</sup>Department of Radiation Oncology, University of Michigan School of Medicine, Ann Arbor, MI, USA. <sup>4</sup>Department of Pathology, University of Michigan School of Medicine, Ann Arbor, MI, USA. <sup>5</sup>Michigan Center for Translational Pathology, University of Michigan School of Medicine, Ann Arbor, MI, USA. <sup>6</sup>Cayman Chemical Company, Ann Arbor, MI, USA. <sup>7</sup>Institute for Cancer Genetics, Department of Pathology and Cell Biology, and Herbert Irving Comprehensive Cancer Center, College of Physicians and Surgeons, Columbia University, New York, NY, USA. <sup>8</sup>Department of Obstetrics and Gynecology, University of Michigan School of Medicine, Ann Arbor, MI, USA. <sup>9</sup>Department of Chemical Engineering, University of Texas at Austin, Austin, TX, USA. <sup>10</sup>Department of Molecular Biosciences, University of Texas at Austin, Austin, TX, USA. <sup>11</sup>Department of Computational Medicine & Bioinformatics, University of Michigan School of Medicine, Ann Arbor, MI, USA. <sup>12</sup>Immunogenomics and Precision Oncology Platform, Department of Radiation Oncology, Memorial Sloan Kettering Cancer Center, New York, NY, USA. <sup>13</sup>Howard Hughes Medical Institute, University of Michigan School of Medicine, Ann Arbor, MI, USA. <sup>14</sup>Graduate Program in Immunology, University of Michigan School of Medicine, Ann Arbor, MI, USA. <sup>15</sup>Graduate Program in Cancer Biology, University of Michigan School of Medicine, Ann Arbor, MI, USA. \*e-mail: wzou@med.umich.edu

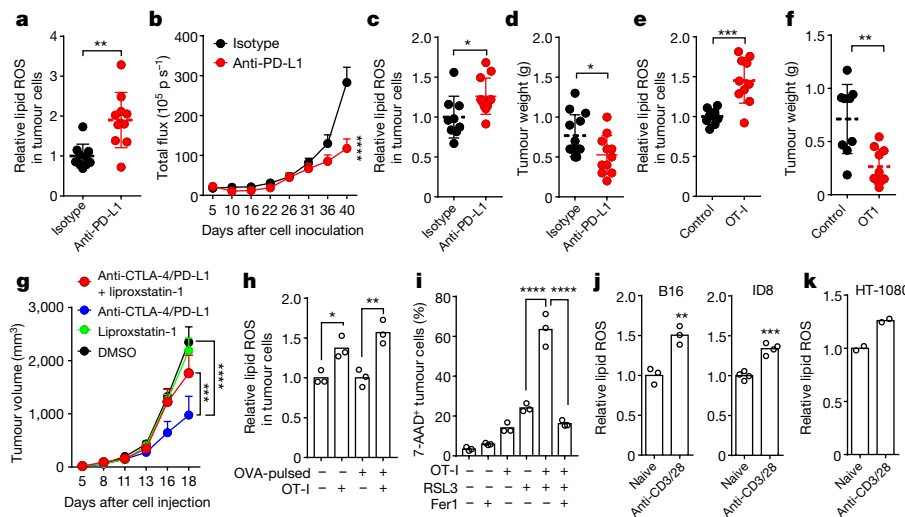


**Fig. 1 | Immunotherapy-activated CD8<sup>+</sup> T cells regulate ferroptosis of cancer cells.** **a, b,** Lipid ROS (**a**) and growth (**b**) of luciferase-expressing ID8 tumours in mice treated with isotype ( $n = 10$ ) or anti-PD-L1 antibody ( $n = 10$ ). **a**, Relative lipid ROS is expressed as the ratio of oxidized to reduced BODIPY-C11 MFI in gated CD45<sup>-</sup> tumour cells. \*\* $P = 0.0014$  (two-tailed  $t$ -test). **b**, Tumour growth was monitored by quantifying total flux (photons per second). \*\*\*\* $P < 0.0001$  on day 40 (two-way ANOVA). Data plotted are mean  $\pm$  s.e.m. **c, d**, Lipid ROS (**c**) and growth (**d**) of B16 tumours in mice treated with isotype or anti-PD-L1 antibody. **c**, Relative lipid ROS was quantified in CD45<sup>-</sup> cells (isotype,  $n = 9$ ; anti-PD-L1,  $n = 11$ ; two-tailed  $t$ -test; \* $P = 0.0274$ ). **d**, Tumour weight was measured on day 17 (isotype,  $n = 13$ ; anti-PD-L1,  $n = 11$ ; two-tailed  $t$ -test; \* $P = 0.0284$ ). **e, f**, Lipid ROS (**e**) and growth (**f**) of OVA<sup>+</sup> B16 tumours in mice treated with OT-I transfusion. **e**, Relative lipid ROS was measured in CD45<sup>-</sup>OVA-H2K<sup>b</sup><sup>+</sup> cells. **f**, Tumour weight was measured on day 14. Control,  $n = 9$ ; OT-I,  $n = 10$ ; \*\*\* $P = 0.0003$  (**e**) and \*\* $P = 0.0013$  (**f**)

(two-tailed  $t$ -test). **g**, Growth of B16 tumours in mice treated with DMSO ( $n = 10$ ), liproxstatin-1 ( $n = 9$ ), anti-CTLA-4 and anti-PD-L1 combination therapy ( $n = 10$ ) or anti-CTLA-4 and anti-PD-L1 plus liproxstatin-1 ( $n = 9$ ). \*\*\* $P = 0.0008$ , \*\*\*\* $P < 0.0001$  (two-way ANOVA). Data plotted are mean  $\pm$  s.e.m. **h**, Relative lipid ROS in B16 or OVA-pulsed B16 cells co-cultured with or without activated OT-I (B16:OT-I ratio of 1:1) for 30 h.  $n = 3$  biological replicates; \* $P = 0.0230$ , \*\* $P = 0.0027$  (one-way ANOVA). **i**, Percentage of 7-AAD<sup>+</sup> B16-OVA cells in co-cultures with OT-I cells (B16:OT-I ratio of 1:1) for 24 h followed by treatment with RSL3 (0.2  $\mu$ M) in the presence of ferrostatin-1 (Fer1; 10  $\mu$ M) for an additional 20 h.  $n = 3$  biological replicates; \*\*\* $P < 0.0001$  (one-way ANOVA). **j, k**, Relative lipid ROS in B16, ID8 (**j**) or HT-1080 (**k**) cells treated with supernatant from naive or activated mouse (**j**) or human (**k**) CD8<sup>+</sup> T cells for 30 h. \*\* $P = 0.0047$ , \*\*\* $P = 0.0002$  (**j**); two-tailed  $t$ -test.  $n = 2$ , T cells were from two donors (**k**).

enhanced the ability of RSL3 to reduce cell viability, and these effects were also abolished by ferrostatin-1 (Extended Data Fig. 2o).

IFN $\gamma$  and tumour necrosis factor (TNF) are cytokines that are released by effector CD8<sup>+</sup> T cells<sup>4,13</sup>. The increase in lipid ROS induced by CD8<sup>+</sup> T-cell supernatant in B16 cells could be abolished by anti-IFN $\gamma$  antibodies, but not by anti-TNF antibodies (Extended Data Fig. 3a). Similarly, IFN $\gamma$  receptor I (IFNGR1)-deficient B16 cells did not show augmented lipid ROS and cell death in response to OT-I cells and CD8<sup>+</sup> T-cell supernatant (Fig. 2a, b, Extended Data Fig. 3b). Treatment with IFN $\gamma$  increased lipid ROS in both mouse B16 and human HT-1080 cells (as assessed by the lipid peroxidation sensor BODIPY-C11; Extended Data Fig. 3c). We also measured lipid ROS using another probe, LiperFluo<sup>14</sup>. B16 and HT-1080 cells showed increased mean fluorescence intensity (MFI) of LiperFluo after IFN $\gamma$  treatment (Extended Data Fig. 3d, e). Pretreatment with IFN $\gamma$  increased the induction of lipid ROS by erastin or RSL3 in B16 (Fig. 2c) and HT-1080 cells (Extended Data Fig. 3f), enhanced cell sensitivity to erastin and RSL3 (Extended Data Fig. 3g, h), and increased the induction of cell death by RSL3 or erastin (Fig. 2d, Extended Data Fig. 3i). Notably, IFN $\gamma$  has been reported to promote erastin-induced cell death in a human melanoma cell line in vitro<sup>15</sup>. In addition, we observed that RSL3- or erastin-induced death of IFN $\gamma$ -primed B16 or HT-1080 cells was blocked by ferrostatin-1 or deferoxamine (DFO) (Extended Data Fig. 3g, h, j, k). A combination of IFN $\gamma$  and RSL3 induced the highest MFI of LiperFluo, and this effect was blocked by ferrostatin-1 (Extended Data Fig. 3e). Moreover, using liquid chromatography with mass spectrometry (LC-MS)<sup>7,8</sup>, we found that IFN $\gamma$  increased oxidized phosphatidylethanolamine (PE) and phosphatidylcholine (PC) (Extended Data Fig. 3l, m) in HT-1080 cells. When combined with RSL3, IFN $\gamma$  further increased oxidized PC in HT-1080 cells (Fig. 2e). In addition to erastin and RSL3, IFN $\gamma$  increased the cell toxicities of several other inducers of ferroptosis—including ML162,

ML210, bathionine sulfoximine (BSO) and sulfasalazine (SAS)—in HT-1080 or B16 cells (Extended Data Fig. 3n–p). When HT-1080 cells were cultured in low concentrations of cystine, IFN $\gamma$  markedly reduced cell viability, and this effect was abolished by ferrostatin-1 (Extended Data Fig. 3q). In vivo, a high dose of IFN $\gamma$  decreased HT-1080 tumour volume in immunodeficient NOD-*scid* IL2R $\gamma$ <sup>null</sup> (NSG) mice, and the anti-tumour effect of IFN $\gamma$  was abolished by liproxstatin-1 (Fig. 2f). In line with this, a low dose of IFN $\gamma$  enhanced the anti-tumour efficacy of SAS in HT-1080 cell-derived tumours in vivo (Extended Data Fig. 3r). We investigated whether T cells themselves are susceptible to inducers of ferroptosis with or without IFN $\gamma$ . Naive human and mouse CD4<sup>+</sup> and CD8<sup>+</sup> T cells were relatively insensitive to cell death induced by erastin or RSL3, regardless of IFN $\gamma$  priming (Extended Data Fig. 4a, b). Neither erastin nor RSL3 impaired IFN $\gamma$  expression in activated human or mouse CD4<sup>+</sup> and CD8<sup>+</sup> T cells (Extended Data Fig. 4c, d). Ferrostatin-1 had no effect on T cell survival or IFN $\gamma$  expression (Extended Data Fig. 4a–d). These data suggest that tumour cells and T cells have different sensitivities to ferroptosis inducers.

To identify biomarkers of cell ferroptosis, we reanalysed data from the Cancer Therapeutics Response Portal (<http://portals.broadinstitute.org/ctrp/>) and evaluated correlations between gene expression profiles across 654 cancer cell lines and cell sensitivities to erastin and RSL3<sup>16</sup>. Overall, we found 16 biomarkers of sensitivity or resistance (Extended Data Fig. 5a). Of those, twelve were highly expressed in cells that were resistant to ferroptosis inducers and four were highly expressed in cells that were sensitive to ferroptosis inducers. *SLC7A11* and *SLC3A2* were exceptionally strongly correlated with resistance to ferroptosis inducers (Extended Data Fig. 5b). We cross-referenced these ferroptosis biomarkers against genes that were differentially expressed after treatment of HT-1080 cells with IFN $\gamma$ . The expression of *SLC7A11* and *SLC3A2* mRNA was reduced by IFN $\gamma$  (Extended Data Fig. 5c). This observation was confirmed by real-time PCR (Extended Data

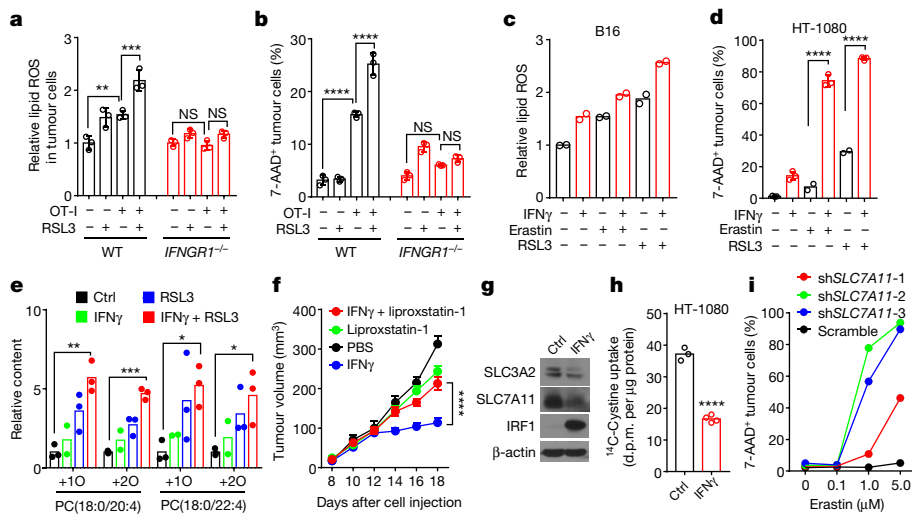


**Fig. 2 | IFN $\gamma$  sensitizes tumour cells to ferroptosis by inhibiting system  $x_c^-$ .** **a, b,** Relative lipid ROS (a) or percentage of 7-AAD $^+$  dead cells (b) in OVA-pulsed wild-type or *IFNGR1* $^{-/-}$  B16 cells co-cultured with OT-I cells (B16:OT-I ratio of 1:1) for 24 h followed by treatment with RSL3 (0.1  $\mu$ M) for an additional 20 h.  $n = 3$  biological replicates. **a**,  $**P = 0.0012$ ,  $***P = 0.0001$ ; NS,  $P = 0.9995$  and 0.4244; **b**,  $****P < 0.0001$ ; NS,  $P = 0.2306$  and 0.7842 (one-way ANOVA). **c**, Relative lipid ROS of B16 cells primed with IFN $\gamma$  (10 ng ml $^{-1}$ ) for 40 h and then treated with erastin (1  $\mu$ M) or RSL3 (0.1  $\mu$ M) for 8 h.  $n = 2$  biological replicates. **d**, The percentage of 7-AAD $^+$  cells among HT-1080 cells primed with IFN $\gamma$  (10 ng ml $^{-1}$ ) for 40 h and then treated with erastin (4  $\mu$ M) or RSL3 (0.05  $\mu$ M) for 20 h.  $n = 2$  or 3 biological replicates;  $****P < 0.0001$  (one-way ANOVA). **e**, Relative content of oxygenated PC species in HT-1080 cells primed with IFN $\gamma$  for 40 h and then treated with RSL3 (0.01  $\mu$ M)

Fig. 5d) and western blotting (Fig. 2g). SLC7A11 and SLC3A2 mediate the exchange of extracellular cystine and intracellular glutamate $^{17}$ . In line with this, IFN $\gamma$  decreased cystine uptake (Fig. 2h) and synergized with the ability of erastin to reduce glutamate release (Extended Data Fig. 5e). In addition, a combination of IFN $\gamma$  and erastin synergistically resulted in the depletion of 90% of intracellular glutathione (GSH) (Extended Data Fig. 5f).

Knockdown of *SLC7A11* in HT-1080 cells increased erastin-induced cell death (Fig. 2i, Extended Data Fig. 5g). By contrast, overexpression of *SLC7A11* rescued erastin-induced cell death and lipid peroxidation in IFN $\gamma$ -primed HT-1080 cells (Extended Data Fig. 5h–j). Similarly, knockdown of *SLC3A2* in HT-1080 cells increased sensitivity to erastin and RSL3 (Extended Data Fig. 5k, l). Supernatant from activated CD8 $^+$  T cells upregulated interferon regulatory factor 1 (IRF1) and downregulated SLC7A11 and SLC3A2 in HT-1080 cells (Extended Data Fig. 5m). Moreover, IFN $\gamma$  inhibited the expression of SLC7A11 and SLC3A2 in human melanoma A375 cells (Extended Data Fig. 5n), and reduced both mRNA and protein expression of SLC7A11 in murine B16 cells (Extended Data Fig. 5o, p). Knockdown of *SLC7A11* in B16 cells resulted in reduced cell viability and increased cell death in the presence of erastin and/or RSL3 (Extended Data Fig. 5q–s).

We then investigated the molecular mechanism by which IFN $\gamma$  inhibited system  $x_c^-$ . The precursor mRNA of *SLC7A11* was rapidly decreased within 2 h of IFN $\gamma$  treatment (Extended Data Fig. 6a), suggesting that it might be transcriptionally regulated. Janus kinase (JAK) and signal transducer and activator of transcription 1 (STAT1) mediate activation of IFN $\gamma$  signalling and regulate the immune response $^{18,19}$ . Two JAK inhibitors, JAK inhibitor I and ruxolitinib, reversed the down-regulation of SLC7A11 and prevented the upregulation of IRF1 induced by IFN $\gamma$  in HT-1080 cells (Extended Data Fig. 6b, c). STAT3 and STAT5 can bind to the *SLC7A11* promoter region and reduce the transcription of *SLC7A11* $^{20}$ . STAT1 chromatin immunoprecipitation (ChIP) followed by quantitative PCR (qPCR) demonstrated that treatment with IFN $\gamma$  enhanced binding of STAT1 to the *SLC7A11* transcription start site

for 10 h.  $n = 3$  biological replicates;  $**P = 0.0016$ ,  $***P = 0.0001$ ,  $*P = 0.0440$  and  $*P = 0.0325$  (one-way ANOVA). **f**, Tumour growth in NSG mice with HT-1080 tumours treated with PBS ( $n = 9$ ), IFN $\gamma$  ( $n = 11$ ), liproxstatin-1 ( $n = 12$ ) or IFN $\gamma$  plus liproxstatin-1 ( $n = 11$ ).  $****P < 0.0001$  (two-way ANOVA). Data plotted are mean  $\pm$  s.e.m. **g**, Immunoblots of SLC7A11, SLC3A2, and IRF1 in HT-1080 cells treated with IFN $\gamma$  (10 ng ml $^{-1}$ ) for 24 h.  $\beta$ -actin serves as loading control. Images are representative of three experiments. **h**,  $^{14}\text{C}$ -Cystine content in IFN $\gamma$ -treated HT-1080 cells incubated in medium supplemented with  $^{14}\text{C}$ -cystine for 45 min.  $n = 3$  or 4 biological replicates;  $****P < 0.0001$  (two-tailed *t*-test). **i**, The percentage of 7-AAD $^+$  dead cells among HT-1080 cells expressing scrambled short hairpin RNA (shRNA) or three individual shRNAs targeting *SLC7A11* (*shSLC7A11-1*, *-2*, *-3*) treated with different concentrations of erastin for 24 h. One of three repeats is shown.

(TSS) in HT-1080 cells (Extended Data Fig. 6d). STAT1 deficiency abolished IFN $\gamma$ -mediated downregulation of SLC7A11 and upregulation of IRF1 (Extended Data Fig. 6e–h) and reversed the induction of lipid peroxidation and erastin- or RSL3-induced cell death in IFN $\gamma$ -primed HT-1080 cells (Extended Data Fig. 6i–k). STAT1 deficiency also reversed RSL3-induced cell death in IFN $\gamma$ -primed mouse B16 cells (Extended Data Fig. 6l).

Cyst(e)inase, an engineered enzyme that degrades cystine as well as cysteine, efficiently induces oxidative stress and results in cell death $^{21,22}$ . Cyst(e)inase induced marked cell death in HT-1080 cells, and this was blocked by three ferroptosis inhibitors (ferrostatin-1, DFO and GSH; Fig. 3a). Cyst(e)inase-induced cell death was further enhanced by priming with IFN $\gamma$  (Fig. 3b). In mouse ID8 and B16 cells, IFN $\gamma$  cooperated with cyst(e)inase to increase lipid peroxidation and induce cell death (Fig. 3c, d, Extended Data Fig. 7a, b). Cell death was prevented by ferrostatin-1 (Extended Data Fig. 7c) and knockout of STAT1 (Extended Data Fig. 7d). We used bovine serum albumin (BSA) and heat-inactivated cyst(e)inase as additional controls, and confirmed that IFN $\gamma$  and cyst(e)inase specifically regulated lipid peroxidation and ferroptosis in tumour cells (Extended Data Fig. 7e, f). We then tested the anti-tumour effects of PD-L1 blockade in combination with cyst(e)inase in vivo. The growth of ID8 cell-derived tumours was similarly reduced in mice treated with either PD-L1 blockade or cyst(e)inase alone, but was strongly inhibited in mice treated with a combination of both (Fig. 3e, Extended Data Fig. 7g). The combination therapy markedly increased lipid peroxidation in tumour cells in vivo (Fig. 3f) and enhanced the percentages of CD8 $^+$  and CD4 $^+$  T cells (Fig. 3g), and the percentages of IFN $\gamma$  $^+$  and TNF $^+$  CD8 $^+$  and CD4 $^+$  T cells in the tumour microenvironment compared to control groups (Fig. 3h, i, Supplementary Fig. 1). Furthermore, the therapeutic efficacy of the combination of cyst(e)inase and PD-L1 blockade was partially reversed by liproxstatin-1 (Extended Data Fig. 7h). These results suggest that cyst(e)inase deprivation by cyst(e)inase can synergize with checkpoint blockade to induce potent anti-tumour immunity by inducing ferroptosis.

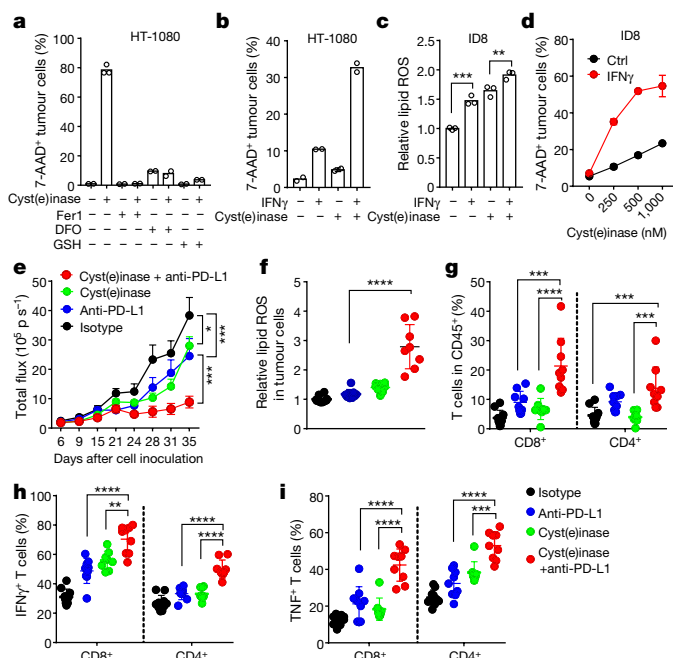


**Fig. 3 | Cyst(e)inase and PD-L1 blockade synergistically induce ferroptosis.** **a**, The percentage of 7-AAD<sup>+</sup> cells among HT-1080 cells treated with cyst(e)inase (1  $\mu$ M) in the presence of ferroptosis inhibitors (Fer1 (10  $\mu$ M), DFO (100  $\mu$ M) or GSH (500  $\mu$ M)) for 24 h.  $n = 2$  or 3 biological replicates. **b**, The percentage of 7-AAD<sup>+</sup> cells among HT-1080 cells primed with IFN $\gamma$  (10 ng ml $^{-1}$ ) for 24 h, and then treated with cyst(e)inase (250 nM) for 24 h.  $n = 2$  biological replicates. **c**, Relative lipid ROS in ID8 cells primed with IFN $\gamma$  for 24 h, and then treated with cyst(e)inase (500 nM) for 12 h.  $n = 3$  biological replicates; \*\*\* $P = 0.0002$ , \*\* $P = 0.0075$  (one-way ANOVA). **d**, The percentage of 7-AAD<sup>+</sup> cells among ID8 cells primed with IFN $\gamma$  for 24 h, then treated with different concentrations of cyst(e)inase for 24 h.  $n = 2$  biological replicates. Data plotted are mean  $\pm$  s.d. **e–i**, Effect of cyst(e)inase in combination with PD-L1 blockade on tumour growth and immune responses. ID8 tumour-bearing mice were treated with isotype antibody ( $n = 10$ ), anti-PD-L1 antibody ( $n = 9$ ), cyst(e)inase ( $n = 8$ ) or cyst(e)inase and anti-PD-L1 ( $n = 9$ ). Tumour growth was monitored over time by quantifying total flux (**e**); relative lipid ROS in CD45<sup>-</sup> ID8 cells (**f**); the percentages of CD8<sup>+</sup> and CD4<sup>+</sup> T cells in CD45<sup>-</sup> cells (**g**); and the percentage of cells expressing IFN $\gamma$  (**h**) and TNF (**i**) in CD8<sup>+</sup> and CD4<sup>+</sup> T cells. \* $P < 0.05$ , \*\* $P < 0.01$ , \*\*\* $P < 0.001$ , \*\*\*\* $P < 0.0001$  (two-way ANOVA (**e**) or one-way ANOVA (**f–i**)). Data plotted in **e** are mean  $\pm$  s.e.m.

We next quantified the number of infiltrating CD8<sup>+</sup> cells and the expression of SLC7A11 and SLC3A2 in human melanoma tissues (Extended Data Fig. 8a). Tumour tissues with higher CD8<sup>+</sup> T cell infiltration had lower levels of SLC7A11 (Fig. 4a) and SLC3A2 (Fig. 4b) on cancer cells. Unexpectedly, in addition to tumour cells, SLC7A11 was highly expressed on CD8<sup>+</sup> T cells, whereas SLC3A2 was basally expressed on tumour cells (Extended Data Fig. 8a). Thus, we focused our subsequent tumour RNA sequencing data analysis on SLC3A2. We examined gene-expression profiles of melanoma patients from The Cancer Genome Atlas (TCGA) (<https://portal.gdc.cancer.gov/>) database. The expression of SLC3A2 negatively correlated with CD8<sup>+</sup> effector T cell signature and IFNG expression (Fig. 4c, d). Kaplan–Meier survival analysis demonstrated that low SLC3A2 expression (Fig. 4e) and high expression of CD8A or IFN $\gamma$  signature (Extended Data Fig. 8b, c) were associated with improved overall survival in patients with melanoma. Furthermore, CD8<sup>+</sup> effector T cell signature (Fig. 4f) and IFNG expression (Fig. 4g) were positively associated with ferroptosis response signature. In addition, we analysed the potential change in SLC3A2 expression in matched melanoma samples from patients before and during treatment with PD-1 blockade<sup>23</sup>. In patients who showed clinical benefit, SLC3A2 expression was reduced but IFNG and CD8A were increased after

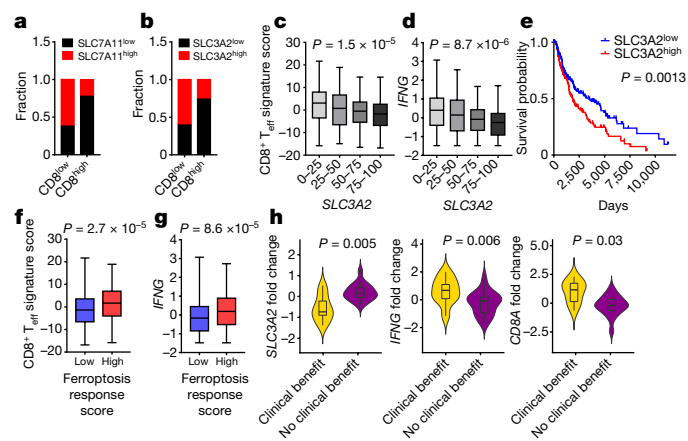


**Fig. 4 | System  $x_c^-$  expression correlates with immune signatures and patient outcome.** **a, b**, Correlation between tumour cell SLC7A11 (**a**) and SLC3A2 (**b**) protein expression and the number of CD8<sup>+</sup> T cells in human melanoma.  $n = 90$ , two-sided Fisher's exact test;  $P = 0.0011$  (**a**);  $P = 0.0052 (**b**). **c, d**, Correlation between SLC3A2 mRNA quartiles and effector CD8<sup>+</sup> T cell signature score (**c**) or IFNG (**d**) in the melanoma TCGA dataset. Data plotted are mean  $\pm$  s.d.  $n = 463$ , one-way ANOVA. **e**, Kaplan–Meier survival curves for patients with melanoma containing low or high expression of SLC3A2 mRNA in the TCGA dataset.  $P$  value is determined by log-rank test. **f, g**, Ferroptosis response signature score is positively associated with effector CD8<sup>+</sup> T cell signature score (**f**) or IFNG (**g**) in melanoma TCGA dataset. **h**, Fold changes in SLC3A2, CD8A and IFNG mRNA in matched pre- and on-therapy samples from patients with melanoma patients who experienced clinical benefit ( $n = 9$ ) or no clinical benefit ( $n = 18$ ). Data plotted are mean  $\pm$  s.d. and  $P$  values are determined by Mann–Whitney test (**f, g, h**).$

the initiation of therapy, compared to patients who did not benefit (Fig. 4h).

In conclusion, we report that immunotherapy-activated CD8<sup>+</sup> T cells promote tumour cell lipid peroxidation and sensitize tumours to ferroptosis through IFN $\gamma$ . Whereas T cells and IFN $\gamma$  sensitize tumour cells to ferroptosis inducers, but may not directly induce tumour cell ferroptosis in a conventional culture system, our in vitro culture with low cystine and in vivo data show that ferroptosis is involved in T cell-mediated cancer immunity. Thus, in addition to apoptosis and senescence, tumour cell ferroptosis is a mechanism for CD8<sup>+</sup> T cell-mediated tumour clearance in vivo. Endogenous mechanism(s) that trigger tumour cell ferroptosis remain to be defined in patients with cancer. Our data suggests that cystine restriction may be a potential endogenous trigger for tumour cell ferroptosis in the tumour microenvironment. Tumour metabolism contributes to immune evasion via inducing T cell dysfunction and exclusion<sup>24,25</sup>. Our work shows how T cell-induced metabolic alterations can affect tumour cell fate. Thus, targeting ferroptosis-associated metabolism in tumours may improve the efficacy of cancer immunotherapy.

## Online content

Any methods, additional references, Nature Research reporting summaries, source data, statements of data availability and associated accession codes are available at <https://doi.org/10.1038/s41586-019-1170-y>.

Received: 24 April 2018; Accepted: 26 March 2019;  
Published online 1 May 2019.

1. Zou, W., Wolchok, J. D. & Chen, L. PD-L1 (B7-H1) and PD-1 pathway blockade for cancer therapy: Mechanisms, response biomarkers, and combinations. *Sci. Transl. Med.* **8**, 328rv4 (2016).
2. Khalil, D. N., Smith, E. L., Brentjens, R. J. & Wolchok, J. D. The future of cancer treatment: immunomodulation, CARs and combination immunotherapy. *Nat. Rev. Clin. Oncol.* **13**, 273–290 (2016).
3. Barry, M. & Bleackley, R. C. Cytotoxic T lymphocytes: all roads lead to death. *Nat. Rev. Immunol.* **2**, 401–409 (2002).
4. Golstein, P. & Griffiths, G. M. An early history of T cell-mediated cytotoxicity. *Nat. Rev. Immunol.* **18**, 527–535 (2018).

5. Dixon, S. J. et al. Ferroptosis: an iron-dependent form of nonapoptotic cell death. *Cell* **149**, 1060–1072 (2012).
6. Yang, W. S. et al. Regulation of ferroptotic cancer cell death by GPX4. *Cell* **156**, 317–331 (2014).
7. Kagan, V. E. et al. Oxidized arachidonic and adrenic PEs navigate cells to ferroptosis. *Nat. Chem. Biol.* **13**, 81–90 (2017).
8. Doll, S. et al. ACSL4 dictates ferroptosis sensitivity by shaping cellular lipid composition. *Nat. Chem. Biol.* **13**, 91–98 (2017).
9. Conrad, M., Angelis, J. P., Vandebaele, P. & Stockwell, B. R. Regulated necrosis: disease relevance and therapeutic opportunities. *Nat. Rev. Drug Discov.* **15**, 348–366 (2016).
10. Linkermann, A. et al. Synchronized renal tubular cell death involves ferroptosis. *Proc. Natl. Acad. Sci. USA* **111**, 16836–16841 (2014).
11. Yang, W. S. & Stockwell, B. R. Ferroptosis: death by lipid peroxidation. *Trends Cell Biol.* **26**, 165–176 (2016).
12. Kim, S. E. et al. Ultrasmall nanoparticles induce ferroptosis in nutrient-deprived cancer cells and suppress tumour growth. *Nat. Nanotechnol.* **11**, 977–985 (2016).
13. Braumüller, H. et al. T-helper-1-cell cytokines drive cancer into senescence. *Nature* **494**, 361–365 (2013).
14. Yamanaka, K. et al. A novel fluorescent probe with high sensitivity and selective detection of lipid hydroperoxides in cells. *RSC Adv.* **2**, 7894–7900 (2012).
15. Tsui, J. et al. Multi-stage differentiation defines melanoma subtypes with differential vulnerability to drug-induced iron-dependent oxidative stress. *Cancer Cell* **33**, 890–904.e895 (2018).
16. Rees, M. G. et al. Correlating chemical sensitivity and basal gene expression reveals mechanism of action. *Nat. Chem. Biol.* **12**, 109–116 (2016).
17. Ishimoto, T. et al. CD44 variant regulates redox status in cancer cells by stabilizing the xCT subunit of system xc<sup>-</sup> and thereby promotes tumor growth. *Cancer Cell* **19**, 387–400 (2011).
18. Schroder, K., Hertzog, P. J., Ravasi, T. & Hume, D. A. Interferon- $\gamma$ : an overview of signals, mechanisms and functions. *J. Leukoc. Biol.* **75**, 163–189 (2004).
19. Wang, W. et al. Effector T cells abrogate stroma-mediated chemoresistance in ovarian cancer. *Cell* **165**, 1092–1105 (2016).
20. Linher-Melville, K., Haftchenay, S., Gunning, P. & Singh, G. Signal transducer and activator of transcription 3 and 5 regulate system Xc- and redox balance in human breast cancer cells. *Mol. Cell. Biochem.* **405**, 205–221 (2015).
21. Cramer, S. L. et al. Systemic depletion of L-cyst(e)ine with cyst(e)inase increases reactive oxygen species and suppresses tumor growth. *Nat. Med.* **23**, 120–127 (2017).
22. Alvarez, S. W. et al. NFS1 undergoes positive selection in lung tumours and protects cells from ferroptosis. *Nature* **551**, 639–643 (2017).
23. Riaz, N. et al. Tumor and microenvironment evolution during immunotherapy with nivolumab. *Cell* **171**, 934–949.e915 (2017).
24. Buck, M. D., Sowell, R. T., Kaech, S. M. & Pearce, E. L. Metabolic instruction of immunity. *Cell* **169**, 570–586 (2017).
25. O'Neill, L. A., Kishton, R. J. & Rathmell, J. A guide to immunometabolism for immunologists. *Nat. Rev. Immunol.* **16**, 553–565 (2016).

**Acknowledgements** We thank all members of the Zou laboratory for suggestions. This work was supported in part by NIH/NCI R01 grants (CA217648, CA123088, CA099985, CA193136 and CA152470), and the NIH through the University of Michigan Rogel Cancer Center Support Grant (CA46592) (W.Z.); the NIH/NCI (CA189623) (E.S. and G.G.); Pershing Square Sohn Cancer Research, the PaineWebber Chair, the NIH/NCI (CA205426), the STARR Cancer Consortium, NCI R35 (CA232097), and an NIH/NCI Cancer Center Support Grant (P30 CA008748) (T.A.C.).

**Reviewer information** *Nature* thanks Matthew Albert, Scott Dixon, Valerian Kagan and the other anonymous reviewer(s) for their contribution to the peer review of this work.

**Author contributions** W.W. and W.Z. conceived the project, designed the experiments and wrote the manuscript. W.W. performed most of the experiments with help from A.S., S.W., L.V. and W.S. M. Green performed part of the tumour immunotherapy experiments and data analysis. J.E.C., W.L., J.L. and M.C. performed bioinformatics analysis. M. Gijón, P.D.K. and J.K.J. performed analysis of oxidized phospholipids by LC-MS. P.L., H.X., J.Z., L.V. and H.Z. assisted with tumour xenograft experiments. X.L. performed STAT1 ChIP experiment. G.L. assisted with the generation of knockout cells. I.K. assisted with flow cytometry analysis. C.L., Y.T., E.S. and G.G. contributed reagents. I.K., W.G., R.L., T.S.L., E.S., G.G., T.A.C. and A.C. contributed to discussions and edited the manuscript. W.Z. supervised work and acquired funding.

**Competing interests** G.G. and E.S. are inventors on intellectual property related to cyst(e)inase and hold equity interest in Aeglea Biotherapeutics Inc. T.A.C. is a co-founder of and holds equity in Gritstone Oncology. T.A.C. holds equity in An2H. T.A.C. acknowledges grant funding from Bristol-Myers Squibb, AstraZeneca, Illumina, Pfizer, An2H, and Eisai. T.A.C. has served as a paid advisor for Bristol-Myers Squibb, Illumina, Eisai, and An2H. Memorial Sloan Kettering has licensed the use of tumour mutation burden (TMB) for the identification of patients that will benefit from immune checkpoint therapy to PGDx. Memorial Sloan Kettering and T.A.C. receive royalties as part of this licensing agreement. W.Z. has served as a consultant or advisor for Lycera, NGM, Synlogic, and Henlix.

#### Additional information

**Extended data** is available for this paper at <https://doi.org/10.1038/s41586-019-1170-y>.

**Supplementary information** is available for this paper at <https://doi.org/10.1038/s41586-019-1170-y>.

**Reprints and permissions information** is available at <http://www.nature.com/reprints>.

**Correspondence and requests for materials** should be addressed to W.Z.

**Publisher's note:** Springer Nature remains neutral with regard to jurisdictional claims in published maps and institutional affiliations.

© The Author(s), under exclusive licence to Springer Nature Limited 2019

## METHODS

**Reagents.** Erastin, RSL3, ML162, ML210, ferrostatin-1, liproxstatin-1, JAK inhibitor I and ruxolitinib were purchased from Cayman Chemical. Doxorubicin (Adriamycin) HCl and gemcitabine were purchased from Selleckchem. Deferoxamine mesylate salt, L-glutathione reduced, sulfasalazine, L-buthionine-sulfoximine, 2-mercaptoethanol, and SIINFEKL peptide (OVA 257–264) were purchased from Sigma-Aldrich. Recombinant human IFN $\gamma$  (285-IF) and mouse IFN $\gamma$  (485-MI) were purchased from R&D. BODIPY 581/591 C11, anti-IFN $\gamma$  (XMG1.2) and anti-TNF (MP6-XT22) blocking antibodies were purchased from Thermo Fisher Scientific. Liperfluo was purchased from Dojindo Molecular Technologies. Cyst(e)inase was obtained from the laboratory of E.S. and G.G. (University of Texas at Austin, TX, USA).

**Cell culture.** Human fibrosarcoma cell line HT-1080 (ATCC, CCL-121), melanoma cell line A375 (ATCC, CRL-1619), and mouse melanoma cell line B16-F0 (ATCC, CRL-6322) were purchased from the American Type Culture Collection. Mouse ovarian cancer cell line ID8 was originally from George Coukos. Cell lines were not authenticated, and none of them are on the list of commonly misidentified cell lines (International Cell Line Authentication Committee). All cell lines were tested for mycoplasma contamination by PCR-based method and confirmed negative for mycoplasma. Cells were cultured in RPMI medium supplemented with 10% FBS, except HT-1080 cells, which were cultured in EMEM supplemented with 10% FBS. To generate OVA-expressing mouse tumour cells, B16 cells were transfected with the plasmid pCI-neo-mOVA, a gift from M. Castro (Addgene plasmid #25099), then selected with 1 mg/ml G418 (Thermo Fisher) for 2 weeks.

Human CD8 $^+$  T cells were isolated from peripheral blood mononuclear cells using the EasySep Human CD8 $^+$  T Cell Isolation Kit (Stemcell), and then stimulated with immobilized anti-CD3 (Clone HIT3 $\alpha$ , BD Biosciences) and anti-CD28 (Clone CD28.2, BD Biosciences) antibodies for 3 days. Mouse CD8 $^+$  T cells were isolated from spleen and lymph nodes using EasySep Mouse CD8 $^+$  T Cell Isolation Kit (Stemcell), and then stimulated with anti-CD3 (Clone 145-2C11, BD Biosciences) and anti-CD28 (Clone 37.51, BD Biosciences) antibodies for 3 days. Supernatants were collected by centrifugation at 3,000g for 10 min and filtered at 0.2  $\mu$ M.

**Generation of ferroptosis-resistant tumour cells.** B16-F0 or ID8 cells ( $2 \times 10^6$ ) were seeded in a 10-cm cell culture dish and treated with RSL3 (1  $\mu$ M) or erastin (5  $\mu$ M) for 10 days. Culture medium was changed every 3 days with the fresh medium supplemented with the compound. Surviving clones were collected and further expanded. The responses of these surviving cells to erastin and RSL3 were tested by cell viability assay. Their ferroptosis resistance was confirmed.

**Human specimens.** Peripheral blood mononuclear cells were isolated from healthy donors. All human samples were collected with informed consent and procedures approved by the institutional review board (IRB) of the University of Michigan.

**OT-I cell isolation and co-culture with OVA $^+$  tumour cells.** OT-I mice, C57BL/6-Tg (TcraTcrb) 1100Mjb/J were purchased from The Jackson Laboratory. Spleen was homogenized, and single cells were suspended in 2 ml Red Blood Cell Lysis Buffer (Sigma-Aldrich) for 1 min. The splenocytes were pelleted, washed, and resuspended at  $2 \times 10^6$  cells per ml in RPMI culture medium containing 1  $\mu$ g/ml OVA257–264 peptide, 5  $\mu$ g/ml mouse recombinant IL-2, and 40  $\mu$ M 2-mercaptoethanol. The cells were incubated at 37°C for 5 days.

To set up the co-culture of OT-I and OVA $^+$  tumour cells, splenocytes were collected after 5 days activation. OT-I cells were purified using EasySep mouse CD8 $^+$  T Cell Isolation Kit (Stemcell). B16-OVA cells were seeded overnight; OT-I cells were then added into the culture at different time points. All cells were collected by trypsinization and analysed by flow cytometry.

**Lipid peroxidation assessed by BODIPY-C11 and Liperfluo staining.** Tumour cells (20,000 cells per well) were seeded in 24-well plates. On the day of the experiment, cells were treated with IFN $\gamma$  (10 ng/ml) or 400  $\mu$ l T-cell supernatant and then with ferroptosis inducers. Cells were then collected by trypsinization for staining. For the co-culture of OVA $^+$  tumour cells and OT-I cells, the mixture was collected and resuspended in 100  $\mu$ l FACS buffer. Cells were first stained with anti-CD45 (30-F11) and anti-OVA<sub>257–264</sub>-H2Kb (25-D1.16) antibodies for 10 min at room temperature. To perform BODIPY-C11 staining, cells were resuspended in 1 ml Hanks balanced salt solution (HBSS, Gibco) containing 5  $\mu$ M BODIPY 581/591 C11 and incubated for 15 min at 37°C in a tissue culture incubator. Cells were washed and resuspended in 200  $\mu$ l fresh HBSS, then analysed immediately with a flow cytometer (LSR II, BD Biosciences).

To quantify the lipid peroxidation in samples from animals that received immunotherapy, a single cell suspension was first prepared. For ID8 tumour-bearing mice, the peritoneal cavity was washed with 5–10 ml PBS to collect tumour and immune cells. A small fraction of the cell pellet was resuspended in 1 ml Red Blood Cell Lysis Buffer (Sigma-Aldrich) for 1 min, and washed and stained with anti-CD45 antibody and then with BODIPY 581/591 C11. For B16 tumour-bearing mice, subcutaneous tumour tissue was resected and cut into small pieces, then tumour tissue was mechanically minced against a 100  $\mu$ M cell strainer, and

washed with PBS. The cell mixture was collected. Tumour and immune cells were pre-enriched using density gradient centrifugation (Ficoll, Sigma-Aldrich). The cell pellet was stained with anti-CD45 and anti-OVA<sub>257–264</sub>-H2Kb antibodies, followed by BODIPY 581/591 C11. Cells were strained through a 40- $\mu$ M cell strainer and analysed immediately with a flow cytometer (LSR II).

For BODIPY 581/591 C11 staining, the signals from both non-oxidized C11 (PE channel) and oxidized C11 (FITC channel) were monitored. The ratio of MFI of FITC to MFI of PE was calculated for each sample. In other cases, only the signal from oxidized C11 was monitored and MFI of FITC was calculated. The data were normalized to control samples as shown by the relative lipid ROS.

For Liperfluo staining, cells were treated with IFN $\gamma$  (10 ng/ml) for 24 h followed by ferroptosis inducers for 6 h. Cells were stained with Liperfluo (10  $\mu$ M) for 30 min at 37°C, collected by trypsinization, and analysed immediately with a flow cytometer. In some cases, cells were pre-loaded with 10  $\mu$ M Liperfluo for 1 h at 37°C, followed with the indicated treatments. The fluorescence intensity in FITC channel was monitored.

**Cell death measurement and immune profiling by FACS.** For cell death analysis, cells were treated, collected, and initially stained with specific antibodies, then resuspended in PBS containing 1  $\mu$ g/ml propidium iodide (PI) or 7-aminoactinomycin D (7-AAD) for 5 min, and directly run on a flow cytometer. For cells expressing intracellular fluorescence proteins, cells were resuspended in PBS containing 1  $\mu$ l LIVE/DEAD Fixable Blue Dead Cell Stain (Thermo Fisher Scientific) for 20 min, then analysed.

To quantify T cells and effector T cell cytokine expression, single-cell suspensions were prepared from fresh tumour tissues. T cells were enriched by density gradient centrifugation. For cytokine staining, T cells were incubated in culture medium containing PMA (5 ng/ml), ionomycin (500 ng/ml), brefeldin A (1:1,000) and monensin (1:1,000) at 37°C for 4 h. Anti-CD45 (30-F11), anti-CD90 (53-2.1), anti-CD4 (RM4-5), and anti-CD8 (53-6.7) antibodies were added for 20 min for surface staining. The cells were then washed and resuspended in 1 ml of freshly prepared Fix/Perm solution (BD Biosciences) at 4°C overnight. After being washed with Perm/Wash buffer (BD Biosciences), the cells were stained with anti-TNF (MP6-XT22) and anti-IFN $\gamma$  (XMG1.2) for 30 min, washed, and fixed in 4% formaldehyde (Sigma Aldrich). All samples were read on an LSR II cytometer and analysed with FACS DIVA software v. 8.0 (BD Biosciences).

**Cell proliferation and viability assay.** Tumour cells were collected and seeded into 96-well plates. After adhesion, cells were pre-treated with IFN $\gamma$  (1–10 ng/ml) for 24 h and then treated with the different ferroptosis inducers or inhibitors. To determine the effect of treatment on cell growth and viability, 10% volume of alamar Blue (Bio-Rad) was added directly into the medium and incubated for 4–6 h. Absorbance at wavelengths of 570 nm and 600 nm was measured. The percentage difference in reduction between treated and control cells was calculated using the following equation: Per cent difference between treatment and control (%) = ((117,216  $\times$   $A_{570}$  of treatment) – (80,586  $\times$   $A_{600}$  of treatment)) / ((117,216  $\times$   $A_{570}$  of control) – (80,586  $\times$   $A_{600}$  of control))  $\times$  100.

After calculation, the viability of control cells was 100% and all others were normalized to control and shown as relative cell viability (%).

**Quantitative PCR analysis.** Total RNA was isolated from cells by column purification (Direct-zol RNA Miniprep Kit, Zymo Research) with DNase treatment. cDNA was synthesized using High-Capacity cDNA Reverse Transcription Kit (Thermo Fisher Scientific) with poly-dT or random hexamer primers. Quantitative PCR (qPCR) was performed on cDNA using Fast SYBR Green Master Mix (Thermo Fisher Scientific) on a StepOnePlus Real-Time PCR System (Thermo Fisher Scientific). Gene expression was quantified using the following primers: human GAPDH forward: TGGTATCGTGAAGGACTC; human GAPDH reverse: AGTAGAGGCAGGGATGATG; human SLC7A11 forward: TGCTGGGCTGATTTCATCTTCG; human SLC7A11 reverse: GAAA GGGCAACCATGAAGAGG; human SLC3A2 forward: CTGGTGGCCG TGTCATAATC; human SLC3A2 reverse: GCTCAGGTAATCGAGACGCC; human IRF1 forward: GAGACCCTGGCTAGAGATGC; human IRF1 reverse: CATGGCACAGCGAAAGTTGG; human pre-SLC7A11 forward: TTGCCATCC ATTCACTCCTCA; human pre-SLC7A11 reverse: GCATGTCTTGACCAT CTGGA; human pre-GAPDH forward: TGACATCAAGAAAGGTGGTGA; human pre-GAPDH reverse: CCTGCACTTTTAAGAGCCA; mouse ACTB forward: AGATCAAGATCATTGCTCCTCCT; mouse ACTB reverse: ACGCAG CTCAGTAACAGTCC; mouse GAPDH forward: AGGAGAGTGGTCCCTCGT CC; mouse GAPDH reverse: TGCCGTAGTGGAGTCATAC; mouse SLC7A11 forward: GCTCGTAATCGCCCTGGAG; mouse SLC7A11 reverse: GGAAAATCTGGATCCGGGCA;

Fold changes in mRNA expression were calculated by the  $\Delta\Delta Ct$  method using GAPDH or ACTB as an endogenous control. Results are expressed as fold change by normalizing to the controls.

**Immunoblotting.** Cells were washed in cold PBS and lysed in 1  $\times$  RIPA lysis buffer (Millipore) with 1  $\times$  protease inhibitor cocktail (Roche). Lysates were

incubated on ice for 10 min and cleared by centrifugation at 15,000g for 15 min. Protein concentration was quantified using a BCA protein assay kit (Thermo Fisher). Thirty micrograms total protein was mixed with sample buffer (Thermo Fisher) and denatured at 95°C for 10 min. Sample was separated by SDS-PAGE and transferred to a PVDF membrane (Millipore). Membranes were blocked with 5% w/v non-fat dry milk and incubated with primary antibodies overnight at 4°C and HRP-conjugated secondary antibodies (CST) for 2 h at room temperature. Signal was detected using Clarity and Clarity Max Western ECL Blotting Substrates (Bio-Rad) and captured using ChemiDoc Imaging System (Bio-Rad). Antibodies were as follows: anti-human SLC7A11 (CST, 12691, 1:1,000), anti-human SLC3A2 (CST, 13180, 1:2,000), anti-mouse SLC7A11 (Thermo Fisher, 711589, 1:1,000), anti-mouse ACSL4 (abcam, ab155282, 1:2,000), anti-IRF1 (CST, 8478, 1:2,000), anti-STAT1 (CST, 9175, 1:1,000), anti-GAPDH (CST, 5174, 1:5,000), and anti- $\beta$ -actin (CST, 5125, 1:5,000).

**Radiolabelled cystine uptake assay.** HT-1080 cells (20,000 cells per well) were seeded overnight and treated with IFN $\gamma$  (10 ng/ml) for 24 h. Medium was removed and changed to cystine-free medium. L-<sup>14</sup>C-Cystine (0.2  $\mu$ Ci/ml) was added and incubated for 15–45 min. Cells were washed three times with cold PBS containing 100  $\mu$ M cystine and lysed in 200  $\mu$ l NaOH (100 mM). Lysates were added into 5 ml scintillation fluid and radioactivity was measured with a Beckman liquid scintillation counter. In the meantime, the same number of cells was lysed in 100  $\mu$ l NaOH (100 mM). The quantity of total protein was determined using a BCA Protein Assay kit and used to normalize the radioactivity. Experiments were performed with biological replicates.

**Glutathione quantification.** HT-1080 cells (2,000 cells per well) were seeded into a white 96-well plate with a clear bottom. On the next day, cells were treated with IFN $\gamma$  for 24 h and then with erastin for 6 h. GSH level was measured using a GSH-Glo Glutathione Assay (Promega) kit following the manufacturer's instruction. In brief, after treatment the culture medium was carefully removed, 100  $\mu$ l of 1  $\times$  GSH-Glo Reagent was directly added to each well and followed with 30-min incubation. Then, 100  $\mu$ l of reconstituted Luciferin Detection Reagent was added and mixed. After 15 min, luminescence was measured using a LMax Microplate Reader (Molecular Devices). A standard curve for GSH concentration was generated along with samples and used for calculation. In the meantime, cell viability in another set of wells was measured using a CellTiter-GLO Luminescent Cell Viability Assay (Promega) kit. In brief, a volume of CellTiter-Glo Reagent equal to the volume of cell culture medium present in each well was added and mixed to induce cell lysis. The plate was incubated for 10 min at room temperature. Luminescence was measured using a LMax Microplate Reader. Relative cell viability was calculated in comparison with control group (100% cell viability). GSH concentration in each group was normalized to cell viability.

**Glutamate assay.** The Glutamate Colorimetric Assay Kit (BioVision) was used for detection of extracellular glutamate released into the medium. HT-1080 cells (20,000 cells per well) were seeded overnight and treated with IFN $\gamma$  (10 ng/ml) for 24 h. Cells were incubated in serum-free DMEM containing 5  $\mu$ M Erastin for 1 h. Fifty microlitres of medium was taken for extracellular glutamate measurement.

**MDA assay.** MDA content in tumour tissue was measured using a Thiobarbituric Acid Reactive Substances (TBARS) assay kit (Cayman Chemical, Item Number 10009055) to monitor lipid peroxidation. About 25 mg B16 tumour tissue was homogenized in 250  $\mu$ l RIPA buffer containing protease inhibitors. Tissue homogenates were centrifuged at 1,600g for 10 min at 4°C and 100  $\mu$ l supernatant was used for MDA analysis. In the meantime, the protein concentration of supernatant was determined using a BCA Protein Assay kit after further dilution, and used to normalize the MDA content.

**Analysis of oxidized phospholipids.** HT-1080 cells were treated, collected by trypsinization, and washed with PBS. The cell pellet ( $10^7$  cells) was re-suspended into 500  $\mu$ l 25 mM HEPES (pH 7.4) containing 200  $\mu$ M DTPA and lysed by sonication on ice. Then, 500  $\mu$ l methanol (HPLC grade) was added. Samples were immediately frozen and kept at –80°C. Upon thawing, 1 ng PE (12:0/12:0) and 1 ng PC (18:0/20:4-d<sub>7</sub>) internal standards were added to each sample. Samples were extracted according as described<sup>26</sup>. The organic phase was dried under vacuum and resuspended in 100  $\mu$ l of a mixture of 75% HPLC solvent A (hexanes/isopropanol 30:40, v/v) and 25% solvent B (5 mM ammonium acetate in hexanes/isopropanol/water 30:40:7, v/v/v). Samples (20  $\mu$ l) were then injected into an HPLC system (ExionLC, Sciex) connected to a triple quadrupole mass spectrometer (Triple Quad 6500+, Sciex). Normal phase chromatography was performed using a HILIC HPLC column (Kinetex HILIC 2.6  $\mu$ m, 100 Å, 100  $\times$  2.1 mm, Phenomenex) at a flow rate of 200  $\mu$ l/min. Solvent B was maintained at 25% for 1 min, increased gradually to 60% in 3 min, and then to 95% in 2 min, and was held for 5 min before re-equilibration for 4 min. Mass spectrometric analysis was performed in the negative ion mode using multiple-reaction monitoring (MRM) of specific precursor-product ion *m/z* transitions upon collision-induced dissociation. The precursor negative ions monitored were the molecular ions [M – H]<sup>–</sup> for PE, and the acetate adducts [M + CH<sub>3</sub>COO]<sup>–</sup> for PC. Identity was further verified

by monitoring at the same time, using polarity switching, the positive molecular ions [M + H]<sup>+</sup> for both PC and PE molecular species. The product ions analysed after collision-induced decomposition, and used for data comparison, were the carboxylate anions corresponding to the nonoxidized or oxidized arachidonoyl chains. The specific precursor-product pairs monitored in negative-ion mode and used for quantification were: PE (18:0/20:4), 766/303; PE (18:0/22:4), 794/331; PE (18:0/20:4-OH), 782/319; PE (18:0/22:4-OH), 810/347; PE (18:0/20:4-OOOH), 798/335; PE (18:0/22:4-OOOH), 826/363; PC (18:0/20:4), 868/303; PC (18:0/22:4), 896/331; PC (18:0/20:4-OH), 884/319; PC (18:0/22:4-OH), 912/347; PC (18:0/20:4-OOOH), 900/335; PC (18:0/22:4-OOOH), 928/363; PE(12:0/12:0) internal standard, 578/199 and PC(18:0/20:4-d<sub>7</sub>) internal standard, 875/310. Results are reported as the ratio between the integrated area of each analyte and the integrated area of the corresponding internal standard. The chromatograms of the ion intensities were plotted (ion count versus time) and the areas under the peaks integrated. Data are normalized to protein concentration for each sample.

**Generation of knockout cells.** *STAT1*, *IFNGR1* and *ACSL4* knockout cells were generated using CRISPR technology. The human *STAT1* locus or mouse *ACSL4* locus were targeted using *STAT1* Double Nickase Plasmid (h) (Santa Cruz Biotechnology, sc-40086-NIC) or *ACSL4* Double Nickase Plasmid (m) (Santa Cruz Biotechnology, sc-424503-NIC), respectively. Tumour cells were transfected with the plasmid using Lipofectamine 2000 (Thermo Fisher Scientific). Twenty-four hours after transfection, cells were selected with 10  $\mu$ g/ml puromycin (Santa Cruz Biotechnology) for another 72 h. Single cell clones were selected and expanded in 96-well plates. For mouse *STAT1* and *IFNGR1*, guide RNAs were cloned into the plasmid pSpCas9 (BB)-Puro (Addgene, 62988). B16 cells were transfected with the plasmid using Lipofectamine 2000 and selected with puromycin. Single cell clones were selected and expanded. Guide RNA sequences to target mouse *STAT1* were: GGTGCGAACGAGACATCAT or CCAGTACAGCCGCTTTCTC; Guide RNAs to target mouse *IFNGR1* were: ATTAGAACATTCTCGCTGGTAC or CTTGAACCTGTCTGTATGCT. Knockout clones were identified by immunoblotting. Multiple deficient clones were pooled for the experiments.

**RNA sequencing analysis.** Total RNA was isolated from cells by column purification (Direct-zol RNA Miniprep Kit, Zymo Research) with DNase treatment. The Ribo-Zero Gold rRNA Removal Kit (Illumina) and TruSeq Stranded Total RNA Library Prep Globin kit (Illumina) were used to prepare the library for RNA sequencing. Sequencing was performed by the University of Michigan DNA Sequencing Core, using the Illumina Hi-Seq 4000 platform, paired end, 50 cycles. Data was analysed by the University of Michigan Bioinformatics Core. The quality of the raw reads data for each sample was first evaluated using FastQC (version 0.11.3). The Tuxedo Suite software package was used for alignment, differential expression analysis, and post-analysis diagnostics. In brief, reads were aligned to the reference transcriptome (hg19) using TopHat (version 2.0.13) and a second round of quality control was performed after alignment. Cufflinks/CuffDiff (version 2.2.1) was used for expression quantification, normalization, and differential expression analysis. Locally developed scripts were used to format and annotate the differential expression data output from CuffDiff. Diagnostic plots were generated using the CummeRbund R package.

**Animal experiments.** Six- to eight-week-old female NSG and C57BL/6 mice were obtained from the Jackson Laboratory. All mice were maintained under pathogen-free conditions. For the HT-1080 tumour model, 10<sup>6</sup> tumour cells were subcutaneously injected into the right flank of NSG mice. In liproxstatin-1 rescue experiment, liproxstatin-1 (30 mg/kg) or recombinant human IFN $\gamma$  (7.5  $\times$  10<sup>5</sup> U per mouse) was administered intraperitoneally every day or every three days, respectively. In the sulfasalazine and IFN $\gamma$  combination experiment, sulfasalazine (120 mg/kg) or IFN $\gamma$  (1.5  $\times$  10<sup>5</sup> U per mouse) was administered intraperitoneally every day or every three days, respectively. Tumour diameters were measured using calipers and tumour volume was calculated.

For adoptive transfer of OT-I cells to the B16-OVA model, 10<sup>5</sup> B16-OVA cells were subcutaneously injected into the right flank of C57BL/6 mice. Meanwhile, splenocytes were isolated from OT-I mice, activated by OVA257-264 peptide and expanded in vitro for 5 days. Enriched OT-I cells (5  $\times$  10<sup>6</sup>) were resuspended into 500  $\mu$ l PBS and intravenously injected into tumour-bearing mice. PBS was given to the control group. Tumour diameters and weights were measured using calipers and a balance (Denver Instrument, SI-114), respectively, at the end of the experiment.

For the B16 tumour model, 10<sup>5</sup> B16F0 cells were subcutaneously injected into the right flank of C57BL/6 mice. On day 3, 100  $\mu$ g anti-CTLA-4 (Bio X Cell) plus 100  $\mu$ g anti-PD-L1 (Bio X Cell), 20 mg/kg liproxstatin-1 or both were administered intraperitoneally to each mouse. Antibodies were administered every 3 days and liproxstatin-1 was administered every day. Tumour diameters were measured using calipers.

For the ID8 tumour model, 2  $\times$  10<sup>6</sup> luciferase-expressing ID8 cells were injected into the peritoneal cavity of each female mouse. On day 7, 100  $\mu$ g isotype

control antibody, 100 µg anti-PD-L1 (Bio X Cell), or 1.5 mg PEG-Cyst(e)inase was administered intraperitoneally to each mouse, and this was repeated every 3 days for the duration of the experiment. To monitor tumour progression, 10 min after intraperitoneal injection of 150 mg/kg body mass d-luciferin (Promega), the bioluminescence signal was assessed with the IVIS Spectrum *In vivo* Imaging System (PerkinElmer). Tumour load was calculated based on the total flux (photons per second (p/s)). Animal studies were conducted under the approval of the University of Michigan Committee on Use and Care of Animals. In none of the experiments did xenograft tumour size surpass 2 cm in any two dimensions, and no animal had severe abdominal distension ( $\geq 10\%$  original body weight increase). Sample size was chosen based on preliminary data. After tumour inoculation mice were randomized and assigned to different groups for treatment.

**Immunohistochemistry (IHC) and digital pathology analysis.** The paraffin-embedded human melanoma tissue microarray was purchased from US Biomax. The slides were baked for 60 min at 60 °C, deparaffinized in xylene, and rehydrated through graded concentrations of ethanol in water. The slides were then subjected to antigen retrieval in 1× AR6 or AR9 buffer (PerkinElmer) using microwave treatment. Immunohistochemistry staining was performed using EnVision G|2 Doublestain System (Agilent) with the following modifications. Anti-human CD8 (1: 50 dilution; Agilent DAKO; clone C8/144b) was first applied to the slides, detected using Polymer/HRP and visualized with HIGHDEF blue IHC chromogen (HRP) (Enzo Life Sciences). Anti-human SLC7A11 (1:100 dilution; Cell Signaling Technology; clone D2M7A; Cat 12691S) or SLC3A2 (1:100 dilution; Cell Signaling Technology; clone D3F9D; Cat 47213S) were subsequently applied, detected using rabbit/mouse (LINK) following Polymer/AP, and visualized with HIGHDEF red IHC chromogen (AP, plus) (Enzo Life Sciences). Sections were left to air-dry, mounted with permanent mounting medium and coverslipped.

Bright field images were acquired by an automated slide-scanning platform (Aperio AT2, Leica Biosystems) at a 400 $\times$  magnification. The images were analysed using ImageScope software (Leica Biosystems). The tissue cores were scored manually on a computer screen with high resolution. Any discrepancies were resolved by subsequent consultation with diagnostic pathologists. The number of CD8 $^{+}$  cells in each core (0.79 mm $^2$ ) was counted. Tumour tissues were divided into CD8 $^{\text{low}}$  and CD8 $^{\text{high}}$  on the basis of mean values of CD8 $^{+}$  cell number. SLC7A11 and SLC3A2 were localized on the cell membrane, and were scored using the *H*-score method, which takes the percentage of positive cells (0–100%) and each staining intensity (0–3+) into account. A final score was calculated on a continuous scale between 0 and 300 using the following formula:

$$H\text{-score} = [1 \times (\% \text{ cells } 1+) + 2 \times (\% \text{ cells } 2+) + 3 \times (\% \text{ cells } 3+)]$$

Tumour tissues were divided into low and high SCL7A11 or SLC3A2 expression according to median *H*-scores for each core. Cores from normal scalp, abdomen, and breast skin tissue were used as controls.

**Signature score computation.** We used a previously published gene set to determine effector CD8 $^{+}$  T cell signature<sup>27</sup>. For ferroptosis response signature, we used a gene set that was upregulated by erastin treatment and reversed by co-treatment with  $\beta$ -mercaptoethanol in HT-1080 cells<sup>28</sup>. Signature scores were computed by inverse-normal transformation of gene expression levels across the cohort followed by summation of inverse-normal values for each sample<sup>29</sup>.

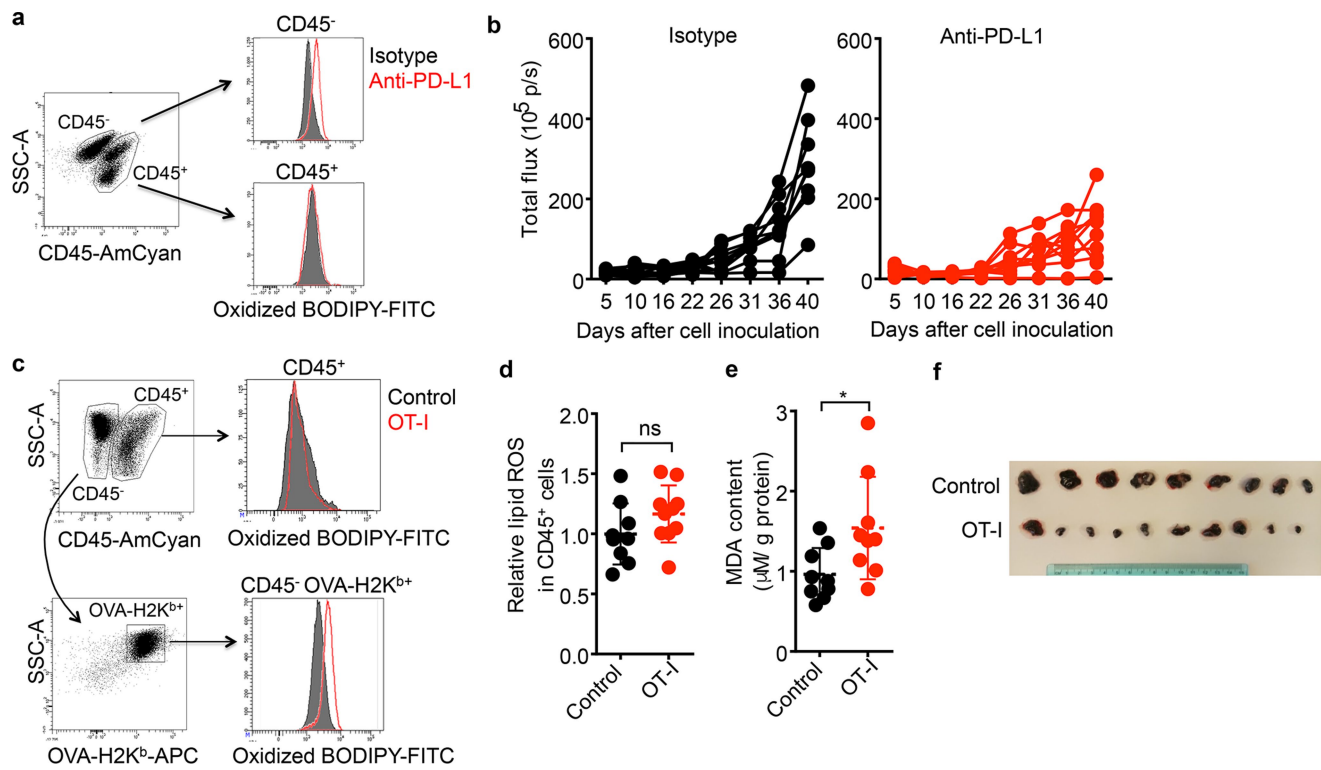
**Statistical analysis.** No statistical methods were used to predetermine sample size. For cell-based experiments, biological triplicates were performed in each single experiment in general, unless otherwise stated. Experiments in Fig. 1a–g, Fig. 3e–i, Extended Data Fig. 1a–f, Extended Data Fig. 2c, f, g, k, l, Extended Data Fig. 7g, h were performed in C57BL/6 mice. Animals were randomized into different groups after tumour cell inoculation and at least ten mice were used for each group, unless otherwise indicated. Animals that failed to develop tumours from the beginning were excluded from the analysis. Experiments in Fig. 2f, Extended Data Fig. 3r were performed in NSG mice. Animals were randomized into different groups after tumour cell inoculation and at least five mice were included in each group. The investigators were not blinded to allocation during experiments and outcome assessment. Data are shown as individual values. Statistical analysis was performed using GraphPad Prism6 software (GraphPad Software, Inc.). Two tailed *t*-tests or Mann–Whitney tests were used to compare treatments with control groups; ANOVA models were used to compare continuous outcomes across multiple experimental groups, and Tukey and Bonferroni corrections were used to adjust *P* values for multiple comparisons, unless otherwise indicated. Inverse-normal signature scores were computed for each sample as previously described. Survival functions were estimated by Kaplan–Meier methods and log-rank test was used to calculate statistical differences. Pearson correlation was used to evaluate the association between expression of two genes.

**Reporting summary.** Further information on research design is available in the Nature Research Reporting Summary linked to this paper.

## Data availability

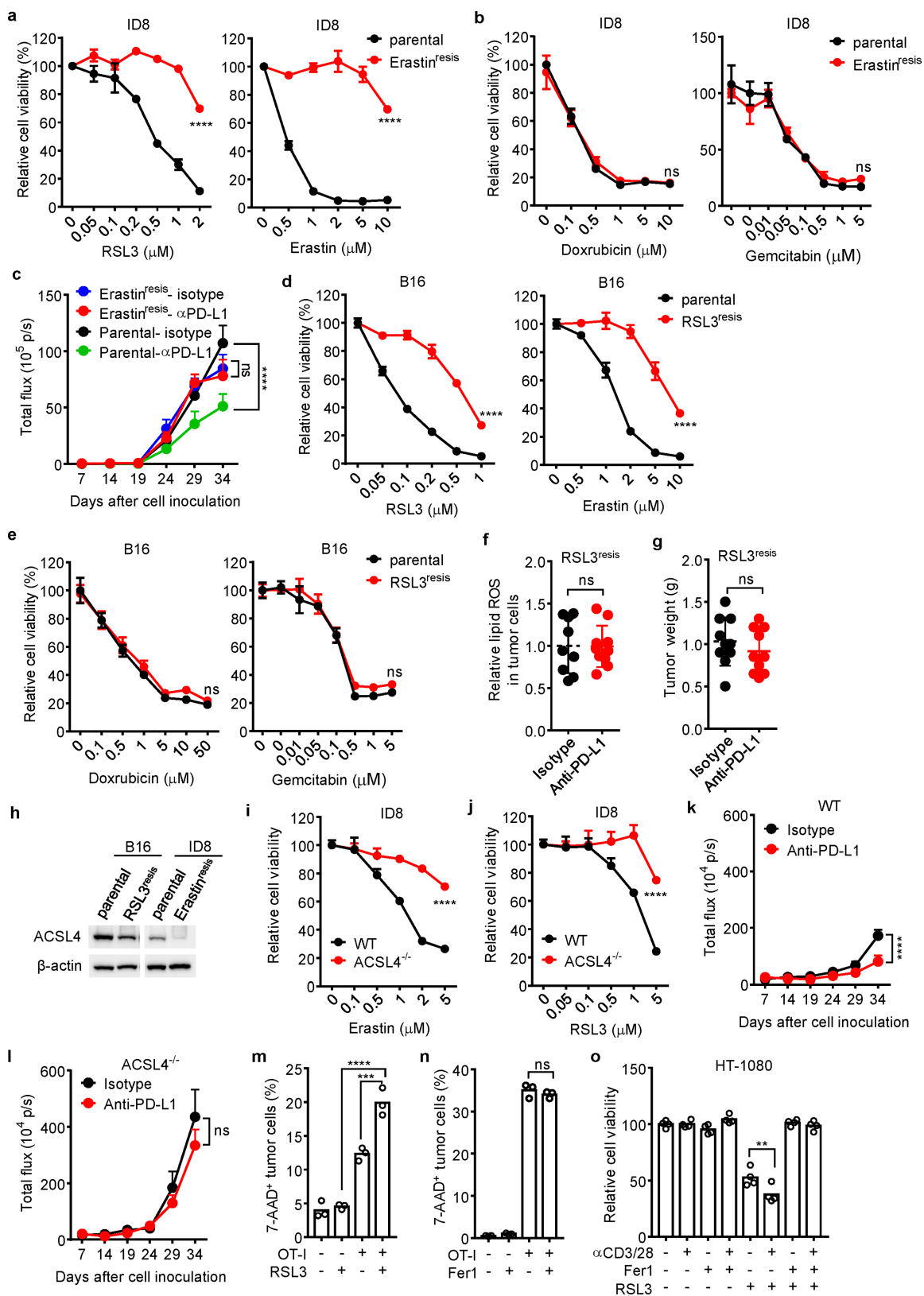
RNA sequencing data that support the findings of this study have been deposited in NCBI Gene Expression Omnibus (GEO) under accession number GSE128392. All other data that supported the findings of this study are available from the corresponding author upon request.

26. Bligh, E. G. & Dyer, W. J. A rapid method of total lipid extraction and purification. *Can. J. Biochem. Physiol.* **37**, 911–917 (1959).
27. Rosenberg, J. E. et al. Atezolizumab in patients with locally advanced and metastatic urothelial carcinoma who have progressed following treatment with platinum-based chemotherapy: a single-arm, multicentre, phase 2 trial. *Lancet* **387**, 1909–1920 (2016).
28. Dixon, S. J. et al. Pharmacological inhibition of cystine–glutamate exchange induces endoplasmic reticulum stress and ferroptosis. *eLife* **3**, e02523 (2014).
29. Wu, Y. M. et al. Inactivation of CDK12 delineates a distinct immunogenic class of advanced prostate cancer. *Cell* **173**, 1770–1782.e1714 (2018).



**Extended Data Fig. 1 | Immunotherapy increases lipid peroxidation in cancer cells.** **a**, Flow cytometry analysis of BODIPY fluorescence in CD45<sup>-</sup> tumour cells isolated from mouse peritoneal cavity. **b**, ID8 tumour growth in individual mice was monitored by quantifying total flux (photons per second). Animals were treated with either anti-PD-L1 or isotype monoclonal antibodies (Fig. 1b). **c**, Flow cytometry analysis of oxidized BODIPY fluorescence in CD45<sup>-</sup> OVA-H2K<sup>b+</sup> tumour cells and CD45<sup>+</sup> cells isolated from subcutaneous B16 tumour tissue. **d**, Relative

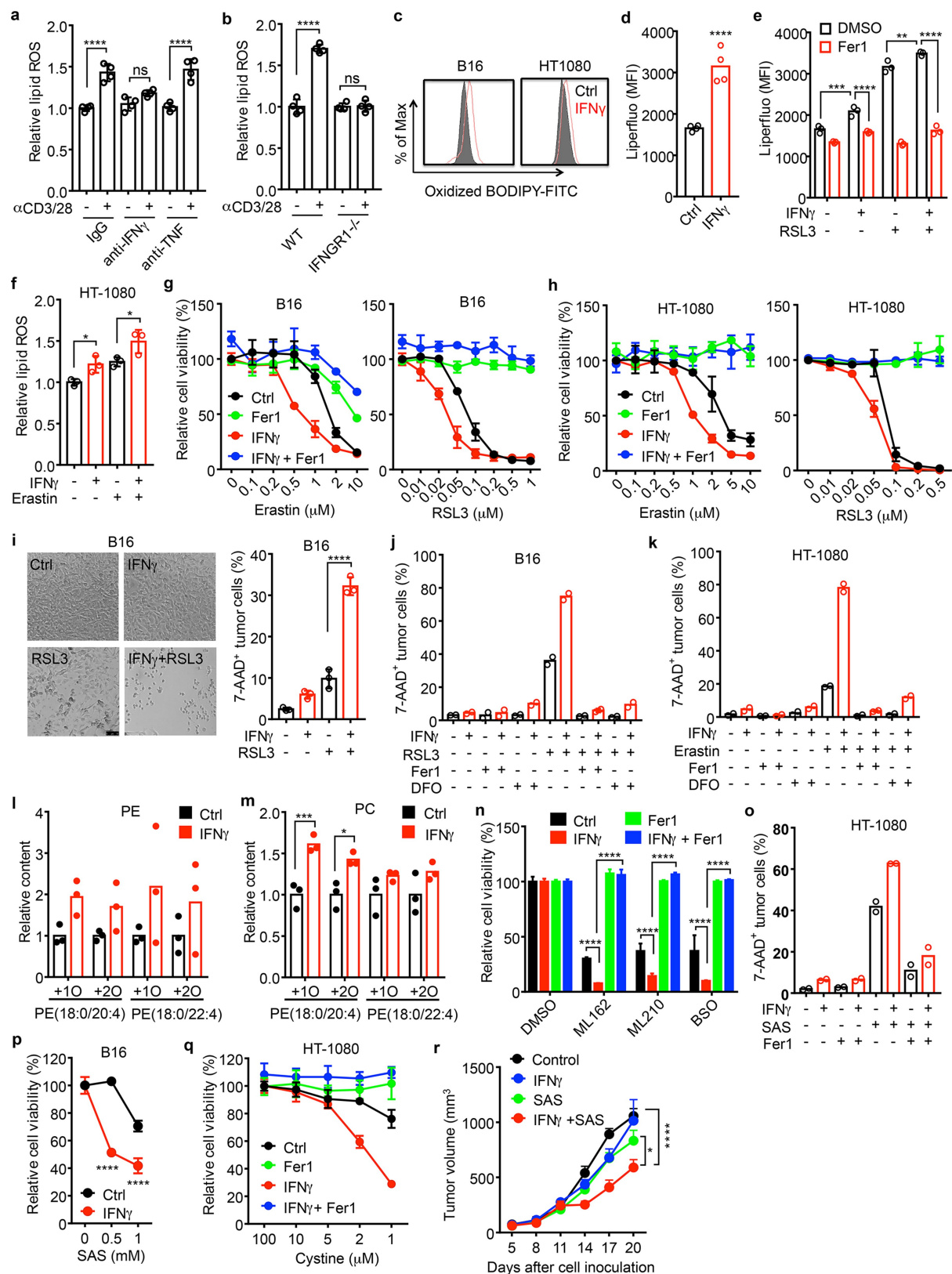
lipid ROS in CD45<sup>+</sup> cells isolated from subcutaneous B16 tumour tissue. Control, n = 9; OT-I, n = 10; ns, P = 0.1584 (two-tailed t-test). **e**, Effect of OT-I cells on MDA concentration in B16 cells in vivo. MDA content in tumour tissue lysate was measured by TBRAS assay and normalized to protein concentration. Control, n = 9; OT-I, n = 9; \*P = 0.0285 (two-tailed t-test). **f**, Subcutaneous B16 tumours from control and OT-I groups were surgically removed and presented. The minimum scale of the rule shows millimetres.



Extended Data Fig. 2 | See next page for caption.

**Extended Data Fig. 2 | Ferroptosis in cancer cells is regulated by immunotherapy and contributes to the anti-tumour effect of immunotherapy.** **a, b,** Relative viability of parental or erastin-resistant ID8 cells treated with different concentrations of the ferroptosis inducers RSL3 or erastin (**a**) or the apoptosis inducers doxorubicin and gemcitabine (**b**) for 24 h.  $n = 3$  or 4 biological replicates (mean  $\pm$  s.d.). \*\*\* $P < 0.0001$  (two-way ANOVA). **c,** Anti-tumour effect of PD-L1 blockade in parental or erastin-resistant ID8 tumour-bearing mice. Mice with luciferase-expressing ID8 tumour cells were treated with anti-PD-L1 or isotype monoclonal antibodies. Tumour growth was monitored by quantifying total flux (photons per second). Parental-isotype,  $n = 8$ ; parental-anti-PD-L1,  $n = 8$ ; erastin<sup>resis</sup>-isotype,  $n = 9$ ; erastin<sup>resis</sup>-anti-PD-L1,  $n = 9$ ; \*\*\* $P < 0.0001$ ; ns,  $P = 0.9018$  (two-way ANOVA). **d, e,** Relative viability of parental B16 or RSL3-resistant B16 cells treated with different concentrations of ferroptosis inducers RSL3 or erastin (**d**) or apoptosis inducers doxorubicin and gemcitabine (**e**) for 24 h.  $n = 3$  or 4 biological replicates (mean  $\pm$  s.d.). \*\*\* $P < 0.0001$  (two-way ANOVA). **f, g,** Effect of anti-PD-L1 therapy on tumour lipid ROS (**f**) and tumour growth (**g**) in RSL3-resistant (RSL3<sup>resis</sup>) B16 tumour bearing mice. Mice with subcutaneous tumours were treated with either anti-PD-L1 or isotype monoclonal antibodies. **f,** Relative lipid ROS in tumour cells was measured by FACS in gated CD45<sup>-</sup> cells (isotype,  $n = 9$ ; anti-PD-L1,  $n = 10$ ; two-tailed *t*-test; ns,  $P = 0.9608$ ). **g,** Tumour weight was measured on day 17

(isotype,  $n = 10$ ; anti-PD-L1,  $n = 10$ ; two-tailed *t*-test; ns,  $P = 0.3621$ ). **h,** Immunoblot of ACSL4 in RSL3<sup>resis</sup> B16 and erastin<sup>resis</sup> ID8 cells compared with parental cells. **i, j,** Relative cell viability of wild-type or ACSL4<sup>-/-</sup> ID8 cells treated with different concentrations of erastin (**i**) or RSL3 (**j**) for 24 h.  $n = 3$  or 4 biological replicates (mean  $\pm$  s.d.). \*\*\* $P < 0.0001$  (two-way ANOVA). **k, l,** Anti-tumour effect of PD-L1 blockade in wild-type (**k**) or ACSL4<sup>-/-</sup> (**l**) ID8 tumour-bearing mice. Luciferase-expressing ID8 tumour-bearing mice were treated with either anti-PD-L1 or isotype monoclonal antibodies. Tumour growth was monitored by quantifying total flux (photons per second). WT, isotype,  $n = 10$ ; WT, anti-PD-L1,  $n = 10$ ; ACSL4<sup>-/-</sup>, isotype,  $n = 9$ ; ACSL4<sup>-/-</sup>, anti-PD-L1,  $n = 9$ ; two-way ANOVA, \*\*\* $P < 0.0001$  (**k**); ns,  $P = 0.317$  (**l**). **m,** Percentage of 7-AAD<sup>+</sup> ID8-OVA cells in mixed co-cultures with OT-I cells (ID8:OT-I = 1:1) for 24 h followed by treatment with RSL3 (0.1  $\mu$ M) for 20 h.  $n = 3$  biological replicates. \*\*\* $P = 0.0004$ , \*\*\* $P < 0.0001$  (one-way ANOVA). **n,** Percentage of 7-AAD<sup>+</sup> B16-OVA cells in mixed co-cultures with OT-I cells (B16:OT-I = 1:2) in the presence of Fer1 (10  $\mu$ M) for 40 h.  $n = 3$  biological replicates. ns,  $P = 0.4640$  (one-way ANOVA). **o,** Relative viability of HT-1080 cells primed with supernatant from anti-CD3 and anti-CD28 activated human CD8<sup>+</sup> T cells for 24 h, then treated with RSL3 (0.05  $\mu$ M) in the presence of Fer1 (10  $\mu$ M) for another 16 h.  $n = 4$  biological replicates. \*\* $P = 0.0015$  (one-way ANOVA).

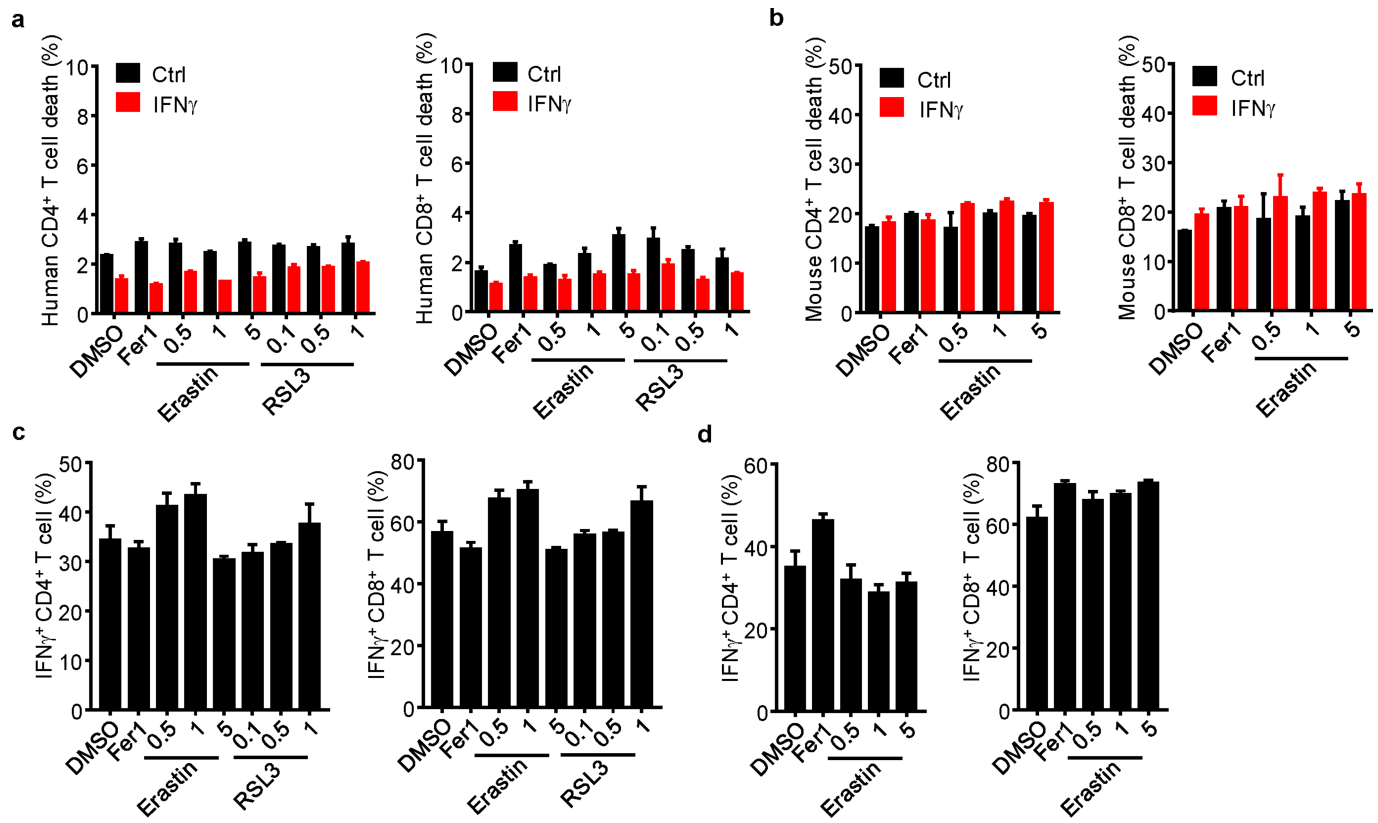


Extended Data Fig. 3 | See next page for caption.

**Extended Data Fig. 3 | IFN $\gamma$  sensitizes tumour cells to ferroptosis.**

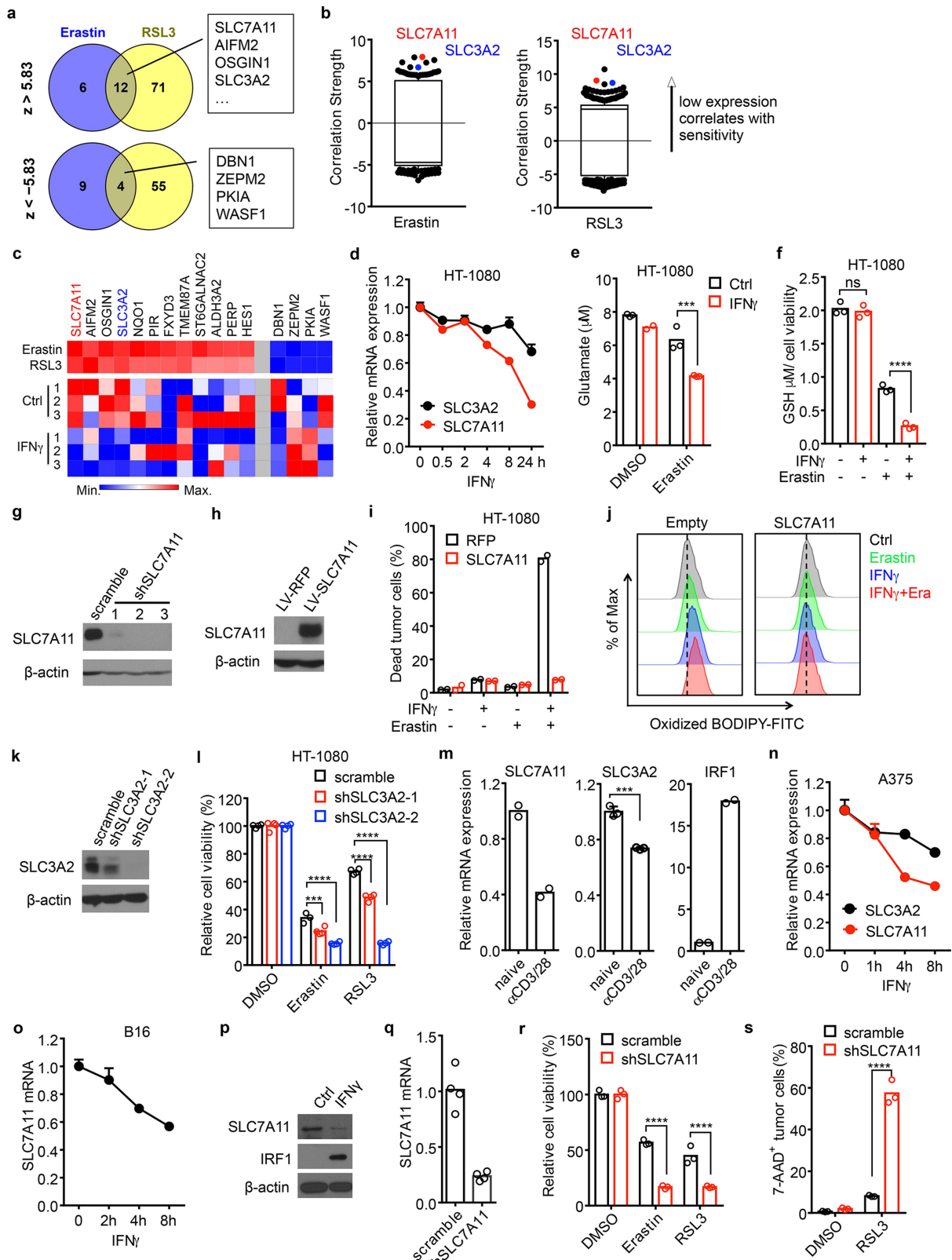
**a**, Relative lipid ROS in B16 cells treated with supernatant from activated CD8 $^{+}$  T cells in the presence of anti-IFN $\gamma$  or anti-TNF blocking antibody for 40 h.  $n = 4$  biological replicates. ns,  $P = 0.1003$ , \*\*\*\* $P < 0.0001$  (one-way ANOVA). **b**, Relative lipid ROS in wild-type or *IFNGRI* $^{-/-}$  B16 cells treated with supernatant from activated CD8 $^{+}$  T cells for 40 h.  $n = 4$  biological replicates. ns,  $P = 0.9981$ , \*\*\*\* $P < 0.0001$  (one-way ANOVA). **c**, Lipid ROS in B16 or HT-1080 cells treated with IFN $\gamma$  for 24 h (representative histogram plot for fluorescence of oxidized BODIPY-C11). **d**, MFI of LiperFluo in B16 cells treated with IFN $\gamma$  for 24 h.  $n = 4$  biological replicates. \*\*\*\* $P < 0.0001$  (two-tailed *t*-test). **e**, MFI of LiperFluo in HT-1080 cells primed with IFN $\gamma$  for 24 h, then treated with RSL3 (0.05  $\mu$ M) for 6 h in the presence of Fer1 (10  $\mu$ M).  $n = 4$  biological replicates. \*\* $P = 0.0067$ , \*\*\* $P = 0.0003$ , \*\*\*\* $P < 0.0001$  (two-way ANOVA). **f**, Relative lipid ROS of HT-1080 cells primed with IFN $\gamma$  (10 ng ml $^{-1}$ ) for 40 h and then treated with erastin (2  $\mu$ M) for 8 h.  $n = 3$  biological replicates. \* $P = 0.0426$  or 0.0250 (one-way ANOVA). **g**, **h**, Relative viability of B16 (**g**) or HT-1080 (**h**) cells primed with or without (Ctrl) IFN $\gamma$  for 40 h in the presence of Fer1 (10  $\mu$ M), followed by treatment with different concentrations of erastin or RSL3 for 24 h.  $n = 3$  or 4 biological replicates (mean  $\pm$  s.d.). **i**, Percentage of 7-AAD $^{+}$  cells among B16 cells primed with IFN $\gamma$  (10 ng ml $^{-1}$ ) for 40 h and then treated with RSL3 (0.1  $\mu$ M) for 20 h. Representative images show cell death (left).  $n = 3$  biological replicates. \*\*\*\* $P < 0.0001$  (one-way

ANOVA). **j**, **k**, Percentage of 7-AAD $^{+}$  cells among B16 (**j**) or HT-1080 (**k**) cells primed with IFN $\gamma$  and then treated with RSL3 (0.1  $\mu$ M, **j**) or erastin (4  $\mu$ M, **k**) in the presence of Fer1 (10  $\mu$ M) or deferoxamine (DFO, 100  $\mu$ M).  $n = 2$  biological replicates. **l**, **m**, Relative content of oxygenated phosphatidylethanolamine (PE) (**l**) and phosphatidylcholine (PC) (**m**) species in HT-1080 cells primed with IFN $\gamma$  (10 ng ml $^{-1}$ ) for 48 h.  $n = 3$  biological replicates. \*\*\* $P = 0.0008$ , \* $P = 0.0167$  (two-tailed *t*-test). **n**, Relative viability of HT-1080 cells primed with IFN $\gamma$  for 24 h, then treated with ML162 (0.1  $\mu$ M), ML210 (0.1  $\mu$ M), or BSO (5  $\mu$ M) for 24 h in the presence of Fer1 (10  $\mu$ M).  $n = 3$  (mean  $\pm$  s.d.), \*\*\*\* $P < 0.0001$  (two-way ANOVA). **o**, Percentage of 7-AAD $^{+}$  cells among HT-1080 cells primed with IFN $\gamma$ , then treated with SAS (0.5 mM) for 40 h in the presence of Fer1 (10  $\mu$ M).  $n = 2$  biological replicates. **p**, Relative viability of B16 cells primed with IFN $\gamma$  for 24 h, then treated with different concentrations of SAS for an additional 24 h.  $n = 3$  (mean  $\pm$  s.d.), \*\*\*\* $P < 0.0001$  (two-way ANOVA). **q**, Relative viability of HT-1080 cells primed with or without IFN $\gamma$ , then cultured with medium supplemented with decreased concentrations of cystine in the presence of Fer1 (10  $\mu$ M) for 20 h.  $n = 3$  or 4 biological replicates (mean  $\pm$  s.d.). **r**, Effect of IFN $\gamma$  and SAS on HT-1080 tumour growth in vivo. HT-1080 cells ( $2 \times 10^6$  cells) were subcutaneously inoculated into NSG mice. Mice were treated either with IFN $\gamma$  ( $1.5 \times 10^5$  U per mouse), SAS (120 mg/kg) or both.  $n = 5$  animals in each group. \* $P < 0.05$ , \*\*\*\* $P < 0.0001$  (two-way ANOVA).



**Extended Data Fig. 4 | Tumour cells and T cells are differentially responsive to ferroptosis inducers.** **a, b**, Percentage of 7-AAD<sup>+</sup> cells in naïve human (**a**) and naïve mouse (**b**) CD4<sup>+</sup> and CD8<sup>+</sup> T cells primed with IFN $\gamma$  (10 ng ml $^{-1}$ ) for 24 h, followed by treatment with Fer1 (10  $\mu$ M) and different concentrations ( $\mu$ M) of erastin and RSL3 for 24 h.  $n = 3$  biological replicates (mean  $\pm$  s.d.). **c, d**, Percentage of IFN $\gamma$ <sup>+</sup> cells in

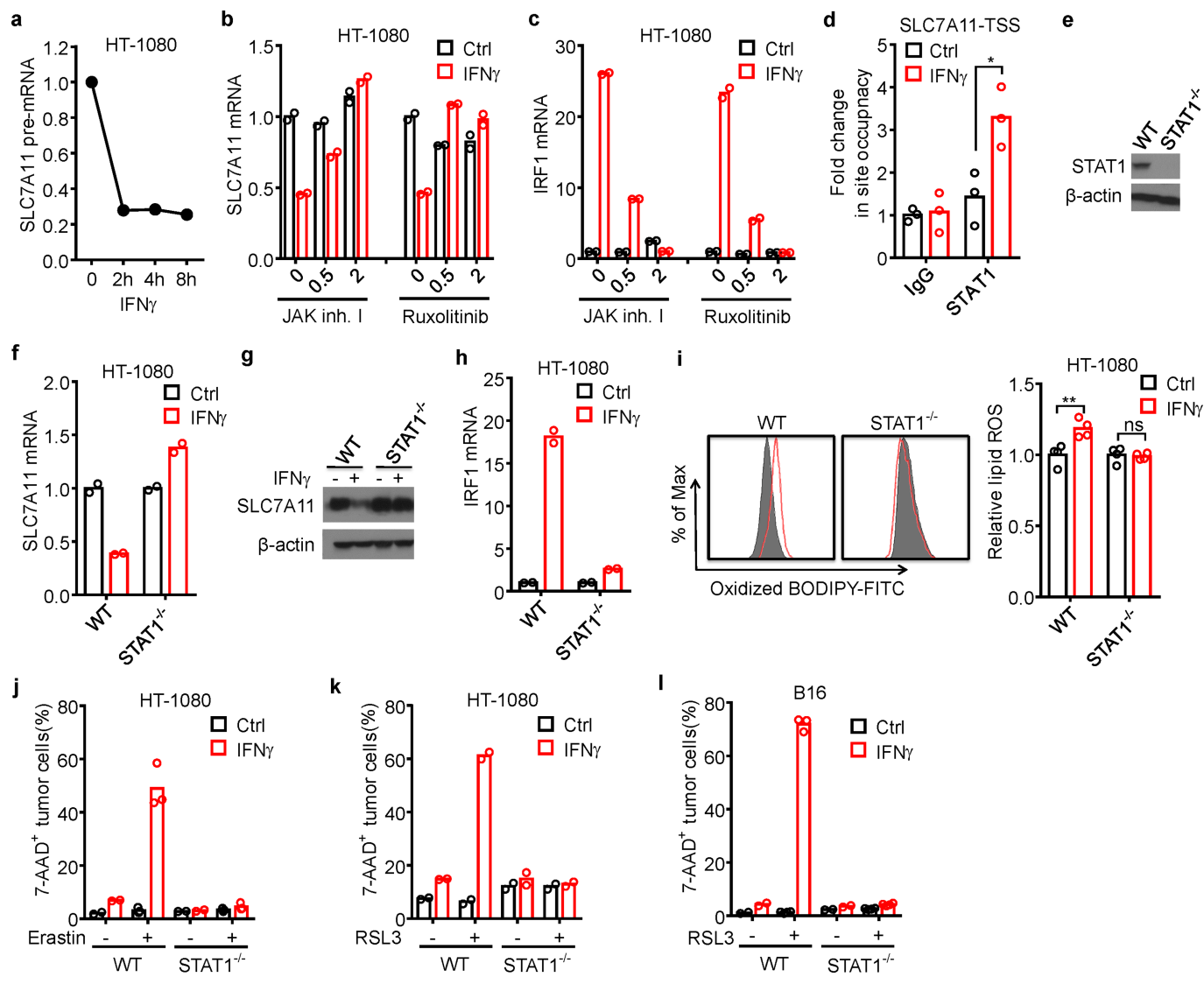
human (**c**) and mouse (**d**) CD4<sup>+</sup> and CD8<sup>+</sup> T cells. T cells were activated with anti-CD3 and anti-CD28 antibodies for 1 day, followed by treatment with Fer1 and different concentrations ( $\mu$ M) of erastin and RSL3 for 2 days. IFN $\gamma$  expression was determined by FACS.  $n = 3$  biological replicates (mean  $\pm$  s.d.).



Extended Data Fig. 5 | See next page for caption.

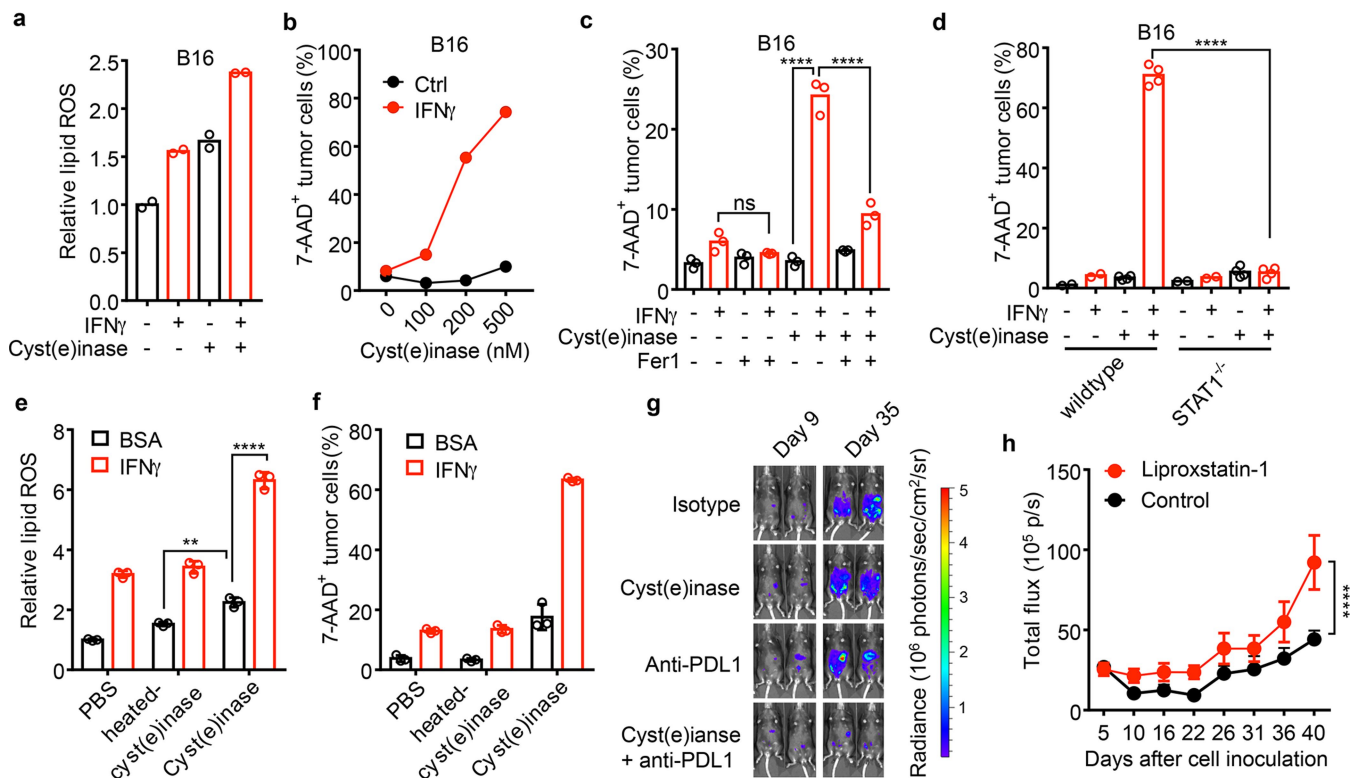
**Extended Data Fig. 5 | IFN $\gamma$  targets system x $_c^-$  to regulate tumour cell ferroptosis.** **a**, Venn diagram showing common genes whose expressions were negatively ( $z > 5.83$ ) or positively ( $z < -5.83$ ) associated with cell line sensitivity to erastin and RSL3. **b**, Box-and-whisker plots show 1st and 99th percentile outlier transcripts (black and coloured dots) whose expression levels are correlated with cell line sensitivity to erastin and RSL3. Plotted values are  $z$ -scored Pearson's correlation coefficients. Line, median; box, 10th–90th percentiles. **c**, Heat maps of the 16 genes associated with sensitivity to erastin and RSL3 and their expressions in IFN $\gamma$ -treated HT-1080 cells (bottom). Left twelve genes are negatively associated with drug sensitivity; right four genes are positively associated with drug sensitivity. **d**, Relative mRNA expression of *SLC3A2* and *SLC7A11* in HT-1080 cells treated with IFN $\gamma$  at different time points.  $n = 3$  biological replicates (mean  $\pm$  s.d.). **e**, Concentration of glutamate released from HT-1080 cells primed with IFN $\gamma$  and then treated with DMSO or erastin.  $n = 3$  biological replicates. \*\*\* $P < 0.001$  (one-way ANOVA). **f**, Intracellular GSH in HT-1080 cells treated with IFN $\gamma$  (10 ng ml $^{-1}$ ) for 24 h and then with erastin (0.5  $\mu$ M) for 16 h.  $n = 3$  biological replicates. ns,  $P = 0.8843$ , \*\*\*\* $P < 0.0001$  (one-way ANOVA). **g, h**, Immunoblots of *SLC7A11* in HT-1080 cells. HT-1080 cells expressed scramble shRNA, one of three independent shRNAs targeting *SLC7A11* (**g**) or lentivector expressing RFP and *SLC7A11* (**h**). **i**, Percentage of dead HT-1080 cells bearing RFP or *SLC7A11* cDNA, primed with or without IFN $\gamma$ , then

treated with or without erastin (5  $\mu$ M) for 20 h.  $n = 2$  biological repeats. **j**, Lipid ROS in HT-1080 cells with empty vector (Empty) or *SLC7A11* cDNA primed with IFN $\gamma$ , then treated with erastin (1  $\mu$ M) for 20 h (representative histogram plot for fluorescence of oxidized BODIPY-C11). **k**, Immunoblots of *SLC3A2* in HT-1080 cells expressing scramble shRNA or either of two independent shRNAs targeting *SLC3A2*. **l**, Relative viability of HT-1080 cells expressing scramble shRNA or shRNA targeting *SLC3A2* (sh*SLC3A2-1, -2*), treated with erastin or RSL3 for 24 h.  $n = 4$  biological replicates; \*\*\* $P < 0.001$ , \*\*\*\* $P < 0.0001$  (two-way ANOVA). **m**, Relative mRNA expression of *SLC7A11*, *SLC3A2*, and *IRF1* in HT-1080 cells treated for 24 h with supernatant from naive or activated CD8 $^+$  T cells. \*\*\* $P < 0.001$  (two-tailed  $t$ -test). **n**, Relative mRNA expression of *SLC3A2* and *SLC7A11* in human A375 cells treated with IFN $\gamma$  at different time points. **o**, Relative mRNA expression of *SLC7A11* in B16 cells treated with IFN $\gamma$  at different time points. **p**, Immunoblots of mouse *SLC7A11* and *IRF1* in B16 cells treated with IFN $\gamma$  (10 ng ml $^{-1}$ ) for 24 h.  $\beta$ -actin serves as loading control. Images are representative of two experiments. **q**, Relative mRNA expression of *SLC7A11* in B16 cells expressing shRNA against *SLC7A11*. **r**, Relative viability of B16 cells expressing scramble shRNA or shRNA targeting *SLC7A11* treated with erastin or RSL3 for 24 h. \*\*\*\* $P < 0.0001$  (two-way ANOVA). **s**, Percentage of 7-AAD $^+$  cells in B16 cells expressing scramble shRNA or shRNA targeting *SLC7A11* treated with RSL3 for 16 h. \*\*\*\* $P < 0.0001$  (one-way ANOVA).



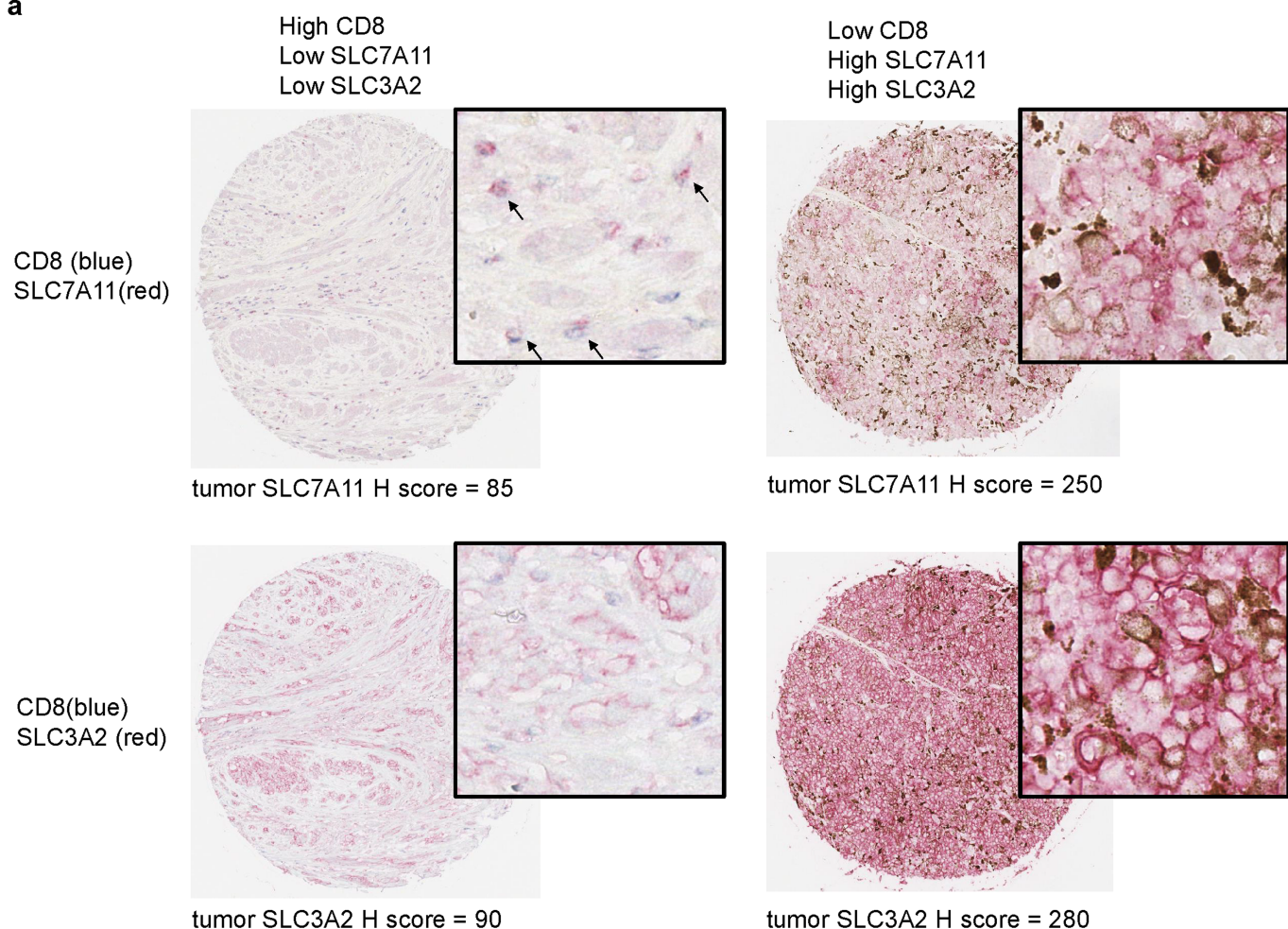
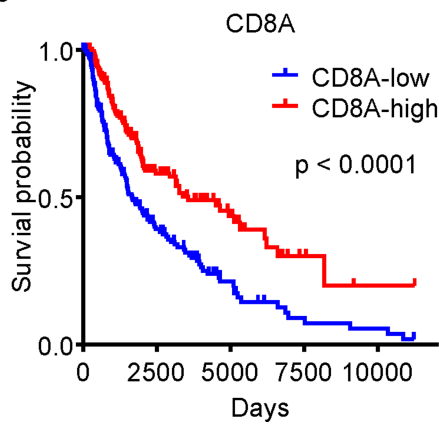
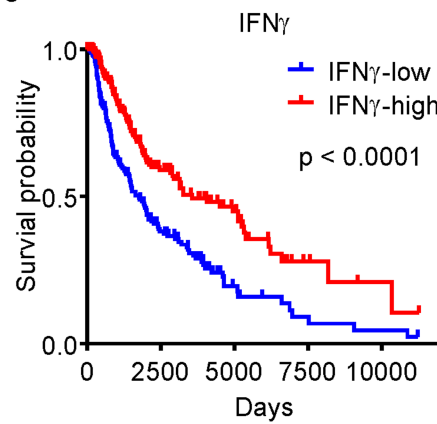
**Extended Data Fig. 6 | IFN $\gamma$  inhibits SLC7A11 through the JAK-STAT1 pathway.** **a**, Relative expression of SLC7A11 pre-mRNA in HT-1080 cells treated with IFN $\gamma$  at different time points. **b, c**, Relative mRNA expression of SLC7A11 (**b**) or IRF1 (**c**) in HT-1080 cells treated with IFN $\gamma$  and JAK inhibitor I or ruxolitinib (0, 0.5 or 2  $\mu$ M) for 24 h. **d**, ChIP of STAT1 in HT-1080 cells treated with or without IFN $\gamma$ . STAT1 binding to SLC7A11 TSS region was quantified by qPCR. Results are expressed as fold change in site occupancy over control. \*P = 0.0156 (two-way ANOVA).

**e**, Immunoblot of STAT1 in wild-type or STAT1 $^{-/-}$  HT-1080 cells generated by CRISPR-Cas9. **f-k**, Wild-type or STAT1 $^{-/-}$  HT-1080 cells treated with or without IFN $\gamma$ . SLC7A11 mRNA level (**f**), SLC7A11 immunoblot (**g**), IRF1 mRNA level (**h**), relative lipid ROS (**i**), erastin-induced cell death (**j**), and RSL3-induced cell death (**k**) were analysed. \*\*P = 0.0033, ns, P > 0.9999 (two-way ANOVA) (**i**, right). **l**, Percentage of 7-AAD $^{+}$  cells in wild-type or STAT1 $^{-/-}$  B16 cells treated with or without IFN $\gamma$ , followed by RSL3 treatment for 24 h. n = 3 biological replicates.



**Extended Data Fig. 7 | Cyst(e)inase and PD-L1 blockade synergistically induce ferroptosis.** **a**, Relative lipid ROS in B16 cells primed with IFN $\gamma$  and then treated with 500 nM cyst(e)inase for 12 h.  $n = 2$  biological repeats. **b**, Percentage of 7-AAD $^{+}$  cells in B16 cells primed with IFN $\gamma$  for 24 h and then treated with different concentrations of cyst(e)inase for 40 h.  $n = 2$  biological repeats. **c**, Percentage of 7-AAD $^{+}$  cells in B16 cells primed with IFN $\gamma$  and then treated with 400 nM cyst(e)inase in the presence of 10  $\mu$ M Fer1 for 24 h.  $n = 3$  biological replicates. ns,  $P = 0.7290$ , \*\*\*\* $P < 0.0001$  (one-way ANOVA). **d**, Percentage of 7-AAD $^{+}$  cells in wild-type or  $STAT1^{-/-}$  B16 cells treated with or without IFN $\gamma$  and then treated with 500 nM cyst(e)inase for 40 h.  $n = 2$  or 4 biological replicates. \*\*\*\* $P < 0.0001$  (one-way ANOVA). **e**, **f**, Relative lipid ROS (e) and percentage of 7-AAD $^{+}$  cells (f) in B16 cells primed with IFN $\gamma$  or BSA,

and then treated with 500 nM heated cyst(e)inase or cyst(e)inase for 24 h (e) or 40 h (f).  $n = 3$  biological replicates. \*\* $P = 0.0023$ , \*\*\*\* $P < 0.0001$  (two-way ANOVA). **g**, Effect of cyst(e)inase combined with PD-L1 blockade on IB8 tumour growth. Tumours were monitored over time by quantifying total flux in mouse peritoneal cavity and bioluminescence imaging of representative mice from indicated days is shown. **h**, Effect of liproxstatin-1 on anti-tumour efficacy of the combination therapy. ID8 tumour-bearing mice treated with a combination of cyst(e)inase and anti-PD-L1 were treated with liproxstatin-1 (10 mg kg $^{-1}$ ,  $n = 9$ ) or DMSO (control,  $n = 9$ ). Tumour growth was monitored over time by quantifying total flux in peritoneal cavity. Data plotted are mean  $\pm$  s.e.m. \*\*\*\* $P < 0.0001$  (two-way ANOVA).

**a****b****c**

**Extended Data Fig. 8 | System  $x_c^-$  expression correlates with immune signatures and patient outcome.** **a**, Representative images of dual staining of CD8 and SLC7A11 (top) or CD8 and SLC3A2 (bottom) by immunohistochemistry in human melanoma samples. The levels of SLC7A11 and SLC3A2 expression on tumour cells were assessed by the

*H*-score method. **b, c**, Kaplan–Meier survival curves for patients with melanoma with low ( $n = 231$ ) or high ( $n = 232$ ) CD8A expression (**b**), and low ( $n = 231$ ) or high ( $n = 232$ ) IFN $\gamma$  signature score (**c**). *P* values determined by log-rank test.

## Reporting Summary

Nature Research wishes to improve the reproducibility of the work that we publish. This form provides structure for consistency and transparency in reporting. For further information on Nature Research policies, see [Authors & Referees](#) and the [Editorial Policy Checklist](#).

### Statistical parameters

When statistical analyses are reported, confirm that the following items are present in the relevant location (e.g. figure legend, table legend, main text, or Methods section).

n/a Confirmed

- The exact sample size (n) for each experimental group/condition, given as a discrete number and unit of measurement
- An indication of whether measurements were taken from distinct samples or whether the same sample was measured repeatedly
- The statistical test(s) used AND whether they are one- or two-sided  
*Only common tests should be described solely by name; describe more complex techniques in the Methods section.*
- A description of all covariates tested
- A description of any assumptions or corrections, such as tests of normality and adjustment for multiple comparisons
- A full description of the statistics including central tendency (e.g. means) or other basic estimates (e.g. regression coefficient) AND variation (e.g. standard deviation) or associated estimates of uncertainty (e.g. confidence intervals)
- For null hypothesis testing, the test statistic (e.g.  $F$ ,  $t$ ,  $r$ ) with confidence intervals, effect sizes, degrees of freedom and  $P$  value noted  
*Give P values as exact values whenever suitable.*
- For Bayesian analysis, information on the choice of priors and Markov chain Monte Carlo settings
- For hierarchical and complex designs, identification of the appropriate level for tests and full reporting of outcomes
- Estimates of effect sizes (e.g. Cohen's  $d$ , Pearson's  $r$ ), indicating how they were calculated
- Clearly defined error bars  
*State explicitly what error bars represent (e.g. SD, SE, CI)*

*Our web collection on [statistics for biologists](#) may be useful.*

### Software and code

Policy information about [availability of computer code](#)

#### Data collection

Flow cytometer BD LSR II was used to run samples and data was acquired and analyzed by BD FACS Diva or FlowJo software. Epoch (BioTek) plate reader was used for requiring absorbance and data was analyzed by Gen5 software. LMax II384 (Molecular Devices) plate reader was used for the assays requiring luminescence quantification and data was analyzed by SoftMax Pro software. GloMax Discover System (Promega) was used for requiring luminescence or fluorescence quantifications. Oxidized phospholipids in cell lysate were analyzed on a HPLC system (ExionLC, Sciex, Framingham, MA) connected to a triple quadrupole mass spectrometer (Triple Quad 6500+, Sciex). Real-time PCR was run on StepOnePlus system (Thermo Fisher) and data was analyzed by StepOne Software v2.2.2. Microscopy pictures were acquired by Leica DMI4000B microscope and analyzed by LAS AF software (Leica Biosystems). Automated slide-scanning was done on Aperio AT2 platform (Leica Biosystems). The images were analyzed with ImageScope software (Leica Biosystems). In vivo bioluminescence signal was assessed and analyzed with the IVIS Spectrum In Vivo Imaging System (PerkinElmer). Microsoft Excel and GraphPad Prism were also used software for data collection and analysis.

#### Data analysis

GraphPad Prism version 7 and R were used for analysis.

For manuscripts utilizing custom algorithms or software that are central to the research but not yet described in published literature, software must be made available to editors/reviewers upon request. We strongly encourage code deposition in a community repository (e.g. GitHub). See the Nature Research [guidelines for submitting code & software](#) for further information.

## Data

Policy information about [availability of data](#)

All manuscripts must include a [data availability statement](#). This statement should provide the following information, where applicable:

- Accession codes, unique identifiers, or web links for publicly available datasets
- A list of figures that have associated raw data
- A description of any restrictions on data availability

RNA sequencing data that support the findings of this study have been deposited in NCBI Gene Expression Omnibus (GEO) under accession number GSE128392. All other data that supported the findings of this study are available from the corresponding author upon request.

## Field-specific reporting

Please select the best fit for your research. If you are not sure, read the appropriate sections before making your selection.

Life sciences       Behavioural & social sciences       Ecological, evolutionary & environmental sciences

For a reference copy of the document with all sections, see [nature.com/authors/policies/ReportingSummary-flat.pdf](http://nature.com/authors/policies/ReportingSummary-flat.pdf)

## Life sciences study design

All studies must disclose on these points even when the disclosure is negative.

Sample size      No statistical method was used to calculate sample size.

Data exclusions      No data was excluded for all in vitro experiments. For animal experiments, if a mouse died due to other condition than tumor burden, it was excluded from the analysis.

Replication      As reported in the figure legends, the findings were reliably reproduced. The anti-PDL1 therapy in ID8-Erastin resistant cells was performed once (Extended Data Fig. 2c). The effect of liproxstatin-1 on the combination of anti-CTLA-4 and anti-PD-L1 (Fig. 1g) was performed once. The anti-PDL1 therapy in ACSL4 knockout ID8 cells was performed once (Extended Data Fig. 2k, l). The effect of liproxstatin-1 on the combination of cyst(e)inase and anti-PDL1 (Extended Data Fig. 7h) was performed once.

Randomization      For all in vivo experiments, animals were randomly assigned into a treatment group after tumor inoculation. The starting tumor burden in the treatment and control groups was similar before treatment.

Blinding      Immunohistochemistry scoring was performed in a blinded way.

## Reporting for specific materials, systems and methods

### Materials & experimental systems

n/a	Involved in the study
<input type="checkbox"/>	<input checked="" type="checkbox"/> Unique biological materials
<input type="checkbox"/>	<input checked="" type="checkbox"/> Antibodies
<input type="checkbox"/>	<input checked="" type="checkbox"/> Eukaryotic cell lines
<input checked="" type="checkbox"/>	<input type="checkbox"/> Palaeontology
<input type="checkbox"/>	<input checked="" type="checkbox"/> Animals and other organisms
<input checked="" type="checkbox"/>	<input type="checkbox"/> Human research participants

### Methods

n/a	Involved in the study
<input checked="" type="checkbox"/>	<input type="checkbox"/> ChIP-seq
<input type="checkbox"/>	<input checked="" type="checkbox"/> Flow cytometry
<input checked="" type="checkbox"/>	<input type="checkbox"/> MRI-based neuroimaging

## Unique biological materials

Policy information about [availability of materials](#)

Obtaining unique materials      Cyst(e)inase can be requested from George Georgiou (gg@che.utexas.edu)

## Antibodies

### Antibodies used

InVivoMAb anti-mouse CTLA-4 (clone 9H10) and anti-mouse PD-L1 (clone 10F. 9G2) were from Bio X Cell.

Antibodies for functional studies: anti-human CD3 (Clone HIT3a, BD Biosciences) and anti-human CD28 (Clone CD28.2, BD Biosciences); anti-mouse CD3 (Clone 145-2C11, BD Biosciences) and anti-mouse CD28 (Clone 37.51, BD Biosciences);

Antibodies used for FACS: anti-CD45 (30-F11, Thermo Fisher Scientific), anti-OVA257-264-H2Kb (25-D1.16, Thermo Fisher Scientific); anti-CD90 (53-2.1, Thermo Fisher Scientific), anti-CD4 (RM4-5, Thermo Fisher Scientific), anti-CD8 (53-6.7, Thermo Fisher Scientific), anti-TNF (MP6-XT22, Thermo Fisher Scientific), anti-IFNy (XMG1.2, Thermo Fisher Scientific)

Antibodies used for immunoblot: anti-human SLC7A11 (CST, Cat#12691), anti-human SLC3A2 (CST, Cat#13180), anti-mouse SLC7A11 (Thermo Fisher Scientific, Cat#711589), anti-IRF1 (CST, Cat#8478), anti-ACSL4 (abcam, Cat#ab155282), anti-GAPDH (CST, Cat#5174), anti-β-actin (CST, Cat#5125), anti-STAT1 (CST, Cat#9175).

### Validation

All antibodies for FACS were well-recognized clones in the field and validated by the manufacturers. These antibodies are further validated and routinely used in our lab.

Antibodies targeting SLC7A11, SLC3A2 and STAT1 were validated by suppression or knockout of the intended target gene by RNAi or CRISPR/Cas9, and verification of the loss of a band of the predicted molecular weight by immunoblotting.

## Eukaryotic cell lines

### Policy information about [cell lines](#)

Cell line source(s)	HT-1080, A375 and B16 are from ATCC. The original source of ID8 is cited.
Authentication	Cell lines were not authenticated.
Mycoplasma contamination	All cell lines in our laboratory are routinely tested for mycoplasma contamination and cells used in this study are negative for mycoplasma.
Commonly misidentified lines (See <a href="#">ICLAC</a> register)	No cell line used in the paper is listed in ICLAC database.

## Animals and other organisms

### Policy information about [studies involving animals; ARRIVE guidelines](#) recommended for reporting animal research

Laboratory animals	Six- to eight-week-old female NOD-scid IL2Rgnull (NSG), C57BL/6-Tg (TcrαTcrβ) 1100Mjb/J (OT-I mice) and wild type C57BL/6 mice were obtained from the Jackson Laboratory. All mice were maintained under pathogen-free conditions.
Wild animals	The study did not involve wild animals.
Field-collected samples	The study did not involve samples collected from field.

## Flow Cytometry

### Plots

Confirm that:

- The axis labels state the marker and fluorochrome used (e.g. CD4-FITC).
- The axis scales are clearly visible. Include numbers along axes only for bottom left plot of group (a 'group' is an analysis of identical markers).
- All plots are contour plots with outliers or pseudocolor plots.
- A numerical value for number of cells or percentage (with statistics) is provided.

### Methodology

#### Sample preparation

For lipid ROS analysis, tumor cells were treated and harvested by trypsinization, resuspended in 1 mL Hanks Balanced Salt Solution (HBSS, Gibco) containing 5 µM BODIPY 581/591 C11 (Thermo Fisher), and incubated for 15 min at 37 °C in a tissue culture incubator. When using LiperFluo, cells were preloaded with Liperfluo and treated with ferroptosis inducers. Cells were then washed and resuspended in 200 µl fresh HBSS and analyzed immediately on a flow cytometer (LSR II, BD Biosciences). For the co-culture of OVA+ tumor cells and OT-I cells, the mixture was collected and resuspended in 100 µl FACS buffer. Cells were firstly stained with anti-CD45 (30-F11) and anti-OVA257-264-H2Kb (25-D1.16) antibodies for 10 minutes at room temperature. To perform BODIPY-C11 staining, cells were resuspended in 1 mL HBSS containing 5 µM BODIPY 581/591 C11 and incubated for 15 minutes at 37°C in a tissue culture incubator. Cells were then washed and resuspended in 200 µl fresh HBSS and analyzed immediately with a flow cytometer.

For cell death analysis, cells were treated, collected and initially stained with specific antibodies, and then resuspended in PBS containing 1 µg/ml Propidium Iodide (PI) or 7-Aminoactinomycin D (7-AAD) for 5 minutes and directly run on a flow cytometer. For cells expressing intracellular fluorescence proteins, cells were resuspended in PBS containing 1 µl LIVE/DEAD Fixable Blue Dead Cell Stain (Thermo Fisher Scientific) for 20 minutes and then analyzed.

To quantify the lipid peroxidation in samples from animals that received immunotherapy, single cell suspension was firstly prepared. For ID8 tumor-bearing mouse, peritoneal cavity was washed with 5 - 10 ml PBS to collect tumor and immune cells. A small fraction of cell pellet was resuspended in 1 ml Red Blood Cell Lysis Buffer (Sigma-Aldrich) for 1 min, washed and stained with anti-CD45 antibody following with BODIPY 581/591 C11. For B16 tumor-bearing mouse, subcutaneous tumor tissue was resected and cut into small pieces, then mechanically disaggregated the minced tumor tissue against a 100 µM cell strainer, washed with PBS to collect the cell mixture. Tumor and inflammatory cells were pre-enriched using density gradient centrifugation (Ficoll, Sigma-Aldrich). Cell pellet was then stained with anti-CD45 and anti-OVA257-264-H2Kb antibodies following with BODIPY 581/591 C11. Cells were strained through a 40 µM cell strainer and analyzed.

To quantify T cell and cytokine production, single-cell suspensions were prepared from fresh tumor tissues and lymphocytes were enriched by density gradient centrifugation. For cytokine staining, lymphocytes were incubated in culture medium containing PMA (5 ng/ml), ionomycin (500 ng/ml), Brefeldin A (1: 1000) and Monensin (1: 1000) at 37°C for 4 hours. Anti-CD45 (30-F11), anti-CD90 (53-2.1), anti-CD4 (RM4-5) and anti-CD8 (53-6.7) were added for 20 minute for surface staining. The cells were then washed and resuspended in 1 ml of freshly prepared Fix/Perm solution (BD Biosciences) at 4°C for overnight. After being washed with Perm/Wash buffer (BD Biosciences), the cells were stained with anti-TNF (MP6-XT22) and anti-IFN $\gamma$  (XMG1.2) for 30 min, washed, and fixed in 4% formaldehyde (Sigma Aldrich).

**Instrument**

All samples were read on an LSR II cytometer (BD Biosciences).

**Software**

All data were analyzed with FACS DIVA software v. 8.0 (BD Biosciences).

**Cell population abundance**

When cells were sorted or enriched, the purity was confirmed by flow cytometry and in each case was above 90% purity.

**Gating strategy**

The cells were gated on FSC-A/SSC-A basis on the location known to contain lymphoid cells and tumor cells. To analyze cell death or lipid peroxidation, CD45 negative population was gated and considered as tumor enriched; when tumor cells expressing OVA, CD45- H2Kb/OVA+ population was gated; The percentage of PI+ population or mean fluorescence intensity of ROS probe were then analyzed in either CD45- or CD45+ population. To analyze cytokine production by T cells, CD45+ population was first gated; and then select CD90+CD8+ or CD90+CD4+ population. In CD8 and CD4 gate, the percentage of TNF+ or IFNg+ cells were analyzed.

Tick this box to confirm that a figure exemplifying the gating strategy is provided in the Supplementary Information.